CLOSE JOURNAL INFORMATION

HELIYON

PublisherName: ELSEVIER SCI LTD

Journal Impact Factor ™

2021	Five Year
3.776	**3.752**

JCR Category	Category Rank	Category Quartile
MULTIDISCIPLINARY SCIENCES *in SCIE edition*	28/74	Q2

Source: Journal Citation Reports 2021. Learn more

Journal Citation Indicator ™

2021	2020
0.72	**0.46**

JCI Category	Category Rank	Category Quartile
MULTIDISCIPLINARY SCIENCES *in SCIE edition*	38/135	Q2

The Journal Citation Indicator is a measure of the average Category Normalized Citation Impact (CNCI) of citable items (articles and reviews) published by a journal over a recent three year period. It is used to help you evaluate journals based on other metrics besides the Journal Impact Factor (JIF).

Learn more

Heliyon 8 (2022) e11990

Contents lists available at ScienceDirect

Heliyon

journal homepage: www.cell.com/heliyon

Research article

Strychnos alkaloids: total synthesis, characterization, DFT investigations, and molecular docking with AChE, BuChE, and HSA

Nesimi Uludag [a], Elvan Üstün [b], Goncagül Serdaroğlu [c,*]

[a] Department of Chemistry, Faculty of Arts and Sciences, Namık Kemal University, 59030, Tekirdag, Turkey
[b] Department of Chemistry, Faculty of Art and Science, Ordu University, 52200 Ordu, Turkey
[c] Sivas Cumhuriyet University, Faculty of Education, Math. and Sci. Edu., 58140, Sivas, Turkey

GRAPHICAL ABSTRACT

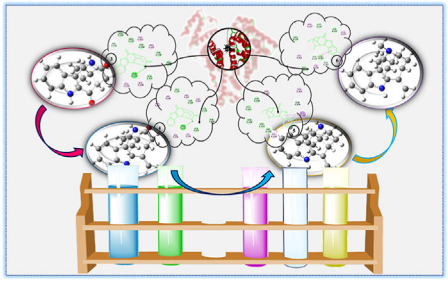

ARTICLE INFO

Keywords:
Uleine
Noruleine
Alzheimer's disease
DFT computations
Molecular dockings

ABSTRACT

An efficient five steps, the protection-deprotection synthetic a novel synthetic routes to(±) noruleine (±)-uleine, are reported starting from tetrahydrocarbazole fused monoalkyl nitrile at C-2 position that is prepared on multigram scale from 2-(3-ethyl-1-oxo-2,3,4,9-tetrahydro-1H-carbazol-2-yl)acetonitrile (1) as well as the key azocino [4,3-*b*]indole skeleton is constructed via the tetrafluoro-1,4-benzoquinone (TFB)-mediated cyclization of a tetrahydrocarbazole derivative possessing direct amide synthesis from nitrile. As a result, Total synthesis of noruleine and uleine has been developed, which is accomplished in 4 and 5- steps synthesis of the ABCD tetracyclic of the strychnos alkaloids with an overall yield of 44% and 39%, respectively. The DFT computations were performed with B3LYP/6-311g(d,p) level to determine inter and intramolecular interactions and reactivity features of the compound **3–6**. Also, TD-DFT computations were performed to characterize the electronic absorption spectra of all compounds. Last, the interactions of compounds **3–6** with selected targets AChE, BuChE, and HSA were evaluated in light of the molecular dockings. The bioactivity and drug-likeness scores revealed that compound 6 3–6 can be proper candidate for future drug-design studies more than the other compounds.

1. Introduction

Uleine-type alkaloid represents a class of the subgroup strychnos alkaloids, and its congeners are defined by the being of the methanoazocino[4,3-*b*]indole carriage an ethyl group at the bridged carbon atom (Scheme 1). Their core structure is also present in some apidospermatan and uleine-type indole alkaloids, including uleine, dasycarpidone, and tubifolidine [1, 2, 3, 4, 5].

* Corresponding author.
E-mail address: goncagul.serdaroglu@gmail.com (G. Serdaroğlu).

https://doi.org/10.1016/j.heliyon.2022.e11990
Received 3 September 2022; Received in revised form 23 October 2022; Accepted 23 November 2022

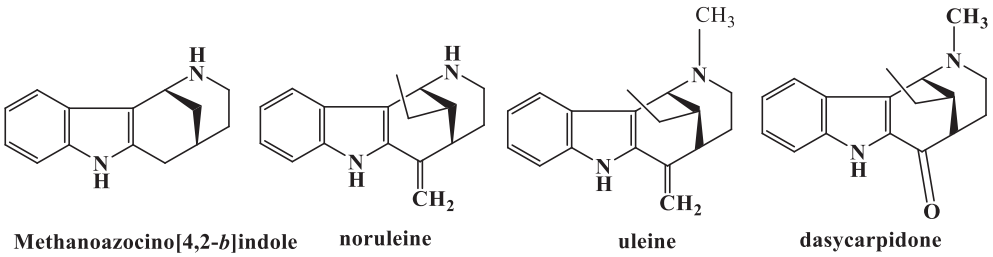

Scheme 1. Structure of uleine-type alkaloids.

Uleine was first isolated from a methanol extract of the rootbarkof *Aspidosperma* uleine Mgf [6, 7, 8]. After the isolation of uleine, Considerable efforts have been devoted to its total synthesis of these structures reported a variety of approaches continuing for a long time [1, 2, 3, 4, 5, 9, 10, 11]. The tetracyclic ring system is believed to be primarily responsible for their drug therapy in Alzheimer's disease, acetylcholinesterase inhibitory activity of uleine, and antimalarial [12, 13, 14, 15, 16, 17]. Furthermore, the methanoazocino[4,3-*b*]indole ring system (ABCD) rings represents an important scaffold in pharmaceutical chemistry, especially for those strychnos-type alkaloids with AIDS [18], anti-inflammatory and analgesic effects [19]. Developing a new method for these structures and bringing them to the literature The development of efficient strategies. To meet such new strategies, we have investigated an approach involving a new approach and a key cyclization reaction tetrafluoro-1,4-benzoquinone (TFB) with a new reagent containing a tetracyclic structure. Uleine and noruleine are a member of strychnos alkaloids including the tetracyclic ring system which are based on the construction of a 1,5-methanoazocino[4,3-*b*]indole skeleton [20, 21, 22, 24, 24] and the presence of the 1,5-methanoazocino[4,3-*b*]indole framework within other similar alkaloids has also prompted the more general development of approaches to this framework [25, 26, 27, 28, 29, 30]. we have previously completed the synthesis of these structures with different reagents for D-rings from the tetrahydocarbazole different substituted groups via an acid catalyst, the DDQ (2,3-Dichloro-5, 6-dicyano-1,4-benzoquinone)-mediated ring closure, intramolecular aldol cyclization, and tetrachloro-1,4-benzoquinone (TCB) as reported previously [31, 32, 33, 34]. Inspired by the results of our work, we used different strategies and developed a new method, that involved direct monoalkylation of tetrahydrocarbazole, that involved a synthesis of D-ring by a different method.

Alternatively, 2-(3-ethyl-1-oxo-2,3,4,9-tetrahydro-1H-carbazol-2-yl) acetonitrile (**1**) allows direct synthetic route to the amide (**2**) [35, 36]. Thus the amide was obtained in one step from the nitrile, due to its simplicity and only in a one-step, this synthesis of the amide improves those previously reported [37]. Such a strategy has never been applied in the synthesis of noruleine and uleine. Firstly, treatment of the keto-amide provided the corresponding alcohol which was subsequently converted into the methylidene-amide (4). Finally, the conversion of noruleine (5) into uleine (6) proved a straightforward matter and simply involved.

This study has two advantages: 1) we directly synthesized the monoalkyl nitrile of the C-2 position of tetrahydrocarbazole and 2) Synthesis of amide directly from nitrile by selecting suitable reagents. Therefore, we planned synthesis of the 1,5-methanoazocino[4,3-*b*]indole (3) compound 3 without the dithiolane protecting group starting from 2-(3-ethyl-1-oxo-2,3,4,9-tetrahydro-1H-carbazol-2-yl)acetonitrile 1 (Scheme 2). The effective structure of the starting cyclization substrates is critical for

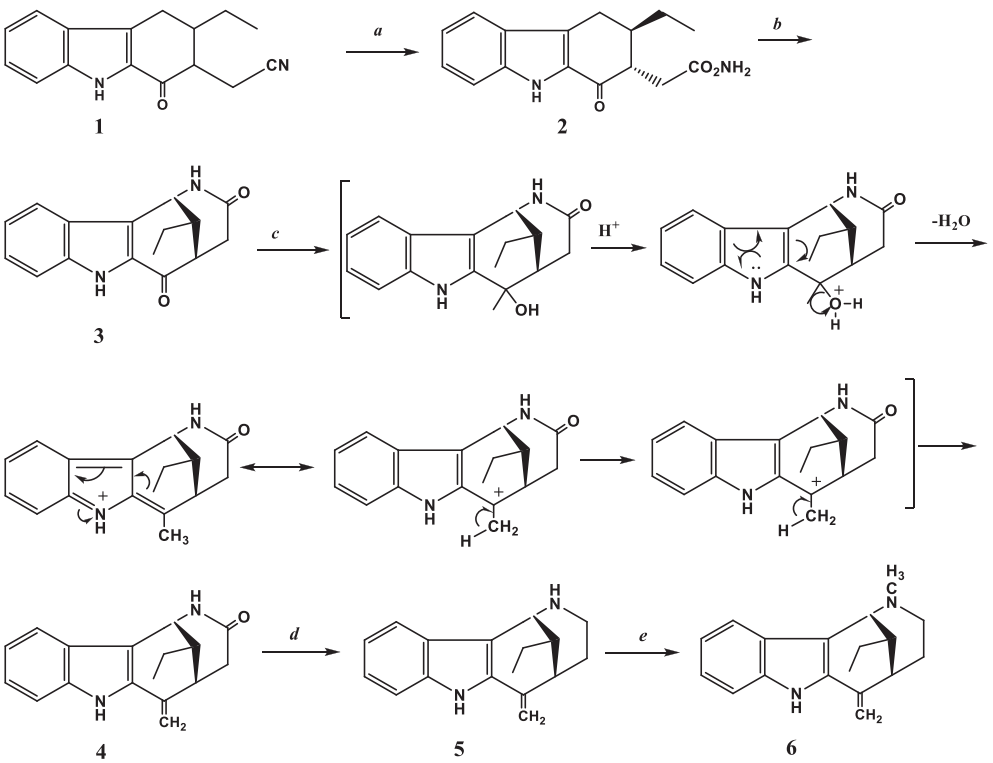

Scheme 2. Synthetic pathway to (±)noruleine and (±)uleine. **a.** TFA-H_2SO_4, 60 °C, 91%; **b.** TFB (Tetrafluoro-1,4-benzoquinone), 50 °C, 83%; **c.** MeLi solution in THF, TFA, 0 °C, 65%; **d.** tris(triphenylphophine)rhodium(1) carbonyl hydride, diphenylsilane, r.t., 93%; **e.** H_2CO (aq), $NaBH_3CN$, r.t., %88.

the achievement of our synthetic plan. For this purpose, this method could be beneficial to the similar synthesis of uleine-type alkaloids, Besides, it is remarkable that we can prepare tetracyclic 1,5-methanoazocino[4,3-*b*]indole **3** to produce in two steps and 74% overall yield. Significantly, our approach does not require protection and deprotection steps in two steps. Transformation of 2-(3-ethyl-1-oxo-2,3,4,9-tetrahydro-1H-carbazol-2-yl)acetonitrile **1** into 2-(2-(aminooxy)-2-oxoethyl)-3-ethyl-2,3,4,9-tetrahydro-1H-carbazol-1-one **2** took place TFA-H_2SO_4 in high yield 91% at room temperature followed by treatment of TFB led to the generation of the azocino[4,3-*b*]indole skeleton **3** [38, 39]. Treatment of the methanoazocino[4,3-*b*]indole **3** with MeLi solution in THF at 0 °C provided the corresponding alcohol which was subsequently converted into 12-ethyl-6-methyliden-1,2,3,4,5,6-hexahydro-1,5-methanoazocino [4,3-b]indole-3-one (4),n 73% yield by adding trifluoroacetic acid [40]. Reduction of **4** with tris(triphenylphosphine)rhodium(I) carbonyl hydride to (±)-noruleine followed by treatment $NaCNBH_3$ in acetonitrile led to (±)-uleine. The conversion of noruleine (5) into uleine (6) proved straightforward matter and simply involved [41, 42, 43]. The work reported here, when considered in conjunction with our previous studies [44, 45, 46], serves to emphasize the considerable utility of both alkylations of tetrahydrocarbazoles (1) and certain cyclization processes, especially when these are applied together within a given synthetic sequence. This kind of method reported has never been applied in the synthesis of uleine-type alkaloids and *strychnos alkaloids* and this synthetic methodology will endure inherent virtues with the accomplishment of our new synthetic method such as with shorter reaction steps and percent efficiency advantage but also a new synthetic pathway routes to azocino[4,3-***b***]indole (**3**).

Alzheimer's Disease (AD) which is possibly associated with a deficiency in cholinergic transmission, is a progressive neurodegenerative disorder that affects the central nervous system [47, 48]. A restricted number of FDA-approved drugs are available for the treatment of AD, which often influences old people and is the most common form of dementia [49]. Inhibition of a certain enzyme is a frequently used strategy in controlling and improving the clinical status of a disease. Managing the amount of Acetylcholine (ACh) which is a neurotransmitter in cholinergic synapses, by using Acetylcholinesterase (AChE) inhibitors is one of the most important therapeutic strategies in the treatment of neurodegenerative diseases [50]. Some drugs currently used in AD treatment (galantamine, donepezil, tacrine, rivastigmine) are AChE inhibitors [51]. Also, when the AChE level is reduced in acute patients, Butyrylcholinesterase (BuChE) could compensate for the AChE to maintain the normal cholinergic pathways [52]. Therefore, dual inhibition of AChE and BuChE is beneficial for the patients.

Nowadays, computational methods have been successfully applied to different kinds of molecular systems because of the importance of understanding the main reasons underlying their observable physical properties of them. Especially, computational tools have been used for looking for the possible power of bio-important molecules as well as the electronic and structural properties [53, 54, 55]. Recently, the azo shiff base molecules like as 2-(((5-mercapto-1,3,4-thiadiazol-2-yl)imino)-methyl)-4-(p-tolyldiazenyl)phenol [56] and 4-((4-hydroxy-3-((pyridine-2-ylimino)methyl)phenyl)diazenyl)benzonitrile [57] were tested on the carbon steel surface to explore the organic corrosion inhibition potency, and the results were supported by quantum chemical computations. Also, the triazole derivatives [58] were studied to explore their possible potency for selective naked-eye sensors for acetate anion, and UV-Vis characteristics were enlighted by TD-DFT computations. In recent work, the possible usage in non-linear optical-dependent technology of triazole derivatives was investigated by computational tools in addition to the electronic and spectroscopic properties [59].

In the present age, organic-based molecules have attracted more and more attention and found application areas, especially in material design, due to their eco-friendliness, in terms of economic and financial management, and the use of natural resources sparingly. For this reason, we aimed to find a short and effective way to synthesize the uleine and noruleine and to explore their possible reactivity features to provide the necessary information in material design. After synthesis and characterization of the compounds studied, DFT-based computations to determine the activity behaviors, and molecular dockings against AChE, BuChE, and HSA were evaluated to explore the alternative molecules being important in bio-medicinal chemistry.

2. Experimental and computational methods

2.1. Material and measurement

^{1}NMR spectra were recorded on 400 MHz a Bruker instrument DPX-400 MHz High-Performance Digital FT-NMR spectrometer using $CDCl_3$ and DMSO-d_6 with tetramethylsilane (TMS) as the international Standard at 25 °C. ^{13} C NMR spectra recorded on 100 MHz instruments. Chemical shifts are reported in parts per million (δ) and the coupling constants are given in Hz. IR spectra were obtained as KBr pellets using a Matson 1000 FT-IR spectrometer. Melting points were determined in a capillary tube on a Gallenkamp apparatus and are uncorrected. Reactions were monitored by thin layer chromatography (silica gel 60 F254). All solvents were used after purification according to international standards.

2.2. Synthesis of the reagents, and products

(3-ethyl-1-oxo-2,3,4,9-tetrahydro-1H-carbazol-2-yl)acetamide (2). A stirred solution of nitrile 1 (5.0 g, 19.8 mmol) was dissolved in 30 mL of TFA-H_2SO_4 (8:2, v/v) and then the mixture was heated at 60 °C for 6 h under a nitrogen atmosphere and then cooled to rt and the mixture was poured into ice-cold water. The resulting mixture was extracted with EtOAc (3 × 60 mL). The combined organic layer separated and was extracted with 10% NaOH. The organic layer was separated and concentrated to give a residue which was purified by column chromatography (*n*-hexane-EtOAc, 4:1) to give an oil, and then the organic layer dried over anhydrous $MgSO_4$, filtered, and concentrated to give a residue which was then recrystallization from diethyl ether to produce compound **2** (4.9 g, 91%), mp 184–186 °C, R_f 0.71 (*n*-hexane). IR spectrum (KBr, ν, cm^{-1}): 3423, 3151, 2970, 2924, 2830, 1693, 1617, 1549, 1410, 1341, 1280, 1132, 1071, 927, 744. ^1H NMR (400 MHz, DMSO-d_6, δ, ppm, J/Hz): 0.93 (t, J = 7.6 Hz, 3H), 1.29–1.41 (m, 1H), 1.52–1.61 (m, 1H), 2.14–2.23 (m, 1H), 2.4 (dd, J = 15.2, 6.3 Hz, 1H), 2.57 (dd, J = 15.2, 4.5 Hz, 1H), 2.67 (dd, J = 16.1, 8.2 Hz, 1H), 2.73–2.84 (m, 1H), 3.16 (dd, J = 16.3, 4.8 Hz, 1H), 6.83 (s, 1H), 7.11 (td, J = 5.8, 0.7 Hz, 1H), 7.33 (td, J = 5.7, 0.7 Hz, 2H), 7.34 (d, td, J = 8.7 Hz, 1H) 7.65 (d, td, J = 8.2 Hz, 1H), 11.44 (br s, 1H, NH-indole). ^{13}C NMR (100 MHz, DMSO-d_6, δ, ppm): 11.7, 22.9, 25.6, 31.7, 42.8, 48.1, 110.4, 117.5, 122.5, 124.3, 124.9, 127.1, 132.2, 137.6, 174.2, 191.8.

Found, %: C, 67.21; H, 6.42; N, 9.84. $C_{16}H_{18}N_2O_3$. Calcd, %: C, 67.12; H, 6.34; N, 9.78.

12-ethyl-1,2,3,4,5,6-hexahydro-1,5-methanoazocino [4,3-b] indole-3,6-dione (3). A stirred solution of the amide 2 (4.0 g, 13.9 mmol) was dissolved in 50 mL of THF. After being stirred for 3 h at rt under nitrogen atmosphere and then the reaction mixture was treated with TFB (Tetrafluoro-1,4-benzoquinone) (3.8 g, 20.8 mmol) in one portion. After being stirred for 6 h at 50 °C. The reaction mixture was quenched with 5 ml of %10 NaOH and extracted with EtOAc (2 × 30 mL), dried over anhydrous $MgSO_4$, and concentrated under pressure. The oil obtained, which was then purified by silica gel chromatography (EtOAc), to give a residue was then recrystallized from diethyl ether to produce compound **3** (2.6 g, 81%), mp 251 °C, R_f 0.73 (EtOAc). IR spectrum (KBr, ν, cm^{-1}): 3241, 3073, 2961, 2917, 2850, 1664, 1611, 1578, 1530, 1429, 1351, 1325, 1242, 1236, 1155, 1132, 980, 618. ^1H NMR (400 MHz, $CDCl_3$, δ, ppm, J/Hz): 0.964 (t, J = 7.4 Hz, 3H), 1.30–1.46 (m, 2H), 2.42–2.55 (m, 2H), 2.87–3.04 (m, 2H), 4.75 (s, 1H), 7.15 (t, J = 7.3 Hz, 1H), 7.35 (d, J = 8.2 Hz, 1H), 7.37 (m, 1H), 7.47 (d, J = 8.3 Hz, 1H), 7.73 (d, J = 8.3 Hz, 1H), 9.51 (s, 1H, NH-indole). ^{13}C NMR (100 MHz, $CDCl_3$, δ, ppm): 11.3,

23.5, 35.6, 44.1, 45.3, 47.9, 112.3, 121.2, 121.8, 124.6, 127.4, 128.3, 128.8, 138.5, 172.2, 191.4.

Found, %: C, 71.72; H, 6.01; N, 10.37. $C_{16}H_{16}N_2O_2$. Calcd, %: C, 71.62; H, 6.01; N, 10.44.

12-Ethyl-6-methyliden-1,2,3,4,5,6-hexahydro-1,5-methanoazocino [4,3-b]indole-3-one (4).

A solution of methylithium (10 mL, 3.0 M MeLi solution in THF) maintained at cooled temperature was treated with a solution of compound **3** (1.5 g, 5.2 mmol) in 30 mL of anhydrous THF under a nitrogen atmosphere at 0 °C. The ensuing solution was stirred at 0 °C for 1 h, then cooled to rt for 1h, and then treated with 30 mL 10% NaOH solution and extracted chloroform, dried over anhydrous $MgSO_4$ and concentrated under pressure, and then the resulting mixture of solution in 40 mL dichloromethane was treated with 10 mL of trifluoroacetic acid. After being stirred for 6 h at rt, the reaction mixture was quenched with 30 mL of 10% Na_2CO_3, dried over anhydrous $MgSO_4$, and concentrated under pressure to give a residue which was then purified by column chromatography (CH_2Cl_2), and was recrystallized from diethyl ether-ethyl acetate (2:1), yielding compound **4** (941 mg, 65%), mp 218–220 °C, R_f 0.56 (EtOAc). IR spectrum (KBr, ν, cm^{-1}): 3254, 3051, 2966, 2913, 2887, 2881, 1654, 1621, 1580, 1544, 1482, 1453, 1404, 1358, 1251, 1222, 1077, 975, 783. ^{1}H NMR (400 MHz, DMSO-d_6, δ, ppm, J/Hz): 0.88 (t, J = 7.5 Hz, 3H), 1.11–1.18 (m, 2H), 2.01–2.09 (m, 1H), 2.16–2.21 (m, 1H), 2.83 (dd, J = 18.4, 7.3 Hz, 1H), 2.93 (d, J = 7.2 Hz, 1H), 4.33 (s, 1H), 5.01 (s, 1H), 5.57 (s, 1H), 7.06 (td, J = 5.6, 0.4 Hz, 1H), 7.18 (td, J = 5.7, 0.9 Hz, 1H), 7.36 (d, J = 8.3 Hz, 1H), 7.54 (d, J = 8.4 Hz, 1H), 8. 22 (d, J = 7.7Hz, 1H), 11.23 (s, 1H, NH-indole). ^{13}C NMR (100 MHz, DMSO-d_6, δ, ppm): 11.4, 22.6, 38.8, 41.5, 43.6, 44.9, 109.2, 112.5, 117.7, 118.1, 118.9, 121.7, 123.7, 130.3, 135.4, 139.1, 172.2.

Found, %: C, 76.57; H, 6.89; N, 10.44. $C_{17}H_{18}N_2O$. Calcd, %: C, 76.66; H, 6.81; N, 10.52.

Noruleine (5). To a mixture of compound 4 (500 mg, 1.9 mmol) and 0.45 g 0.5 mmol), tris(triphenylphophine)rhodium(1) carbonyl hydride was dissolved in 40 mL anhydrous THF. To this solution 0.12 g (0.5 mmol) diphenylsilane added. The whole mixture was stirred for 1 h at rt. The reaction mixture was quenched with EtOAc (2 × 30 mL), dried over anhydrous $MgSO_4$, and concentrated under pressure to give a residue which was then purified by column chromatography (EtOAc-acetone-$N(CH_2CH_3)_3$, 4:1:1), and was recrystallized from diethyl ether-ethyl acetate (2:1), yielding compound **5** (300 mg, 93%), R_f 0.43 (EtOAc). IR spectrum (KBr, ν, cm^{-1}): 3241, 2963, 2922, 1671, 1619, 1457, 1329, 1201, 1166, 1134, 906, 781, 738. ^1H NMR (400 MHz, $CDCl_3$, δ, ppm, J/Hz): 0.79 (t, J = 7.4 Hz, 3H), 0.93–1.58 (m, 2H), 1.63 (d, J = 12.3 Hz, 1H), 1.87–2.29 (m, 3H), 2.31–2.88 (m, 3H), 4.34 (s, 1H), 4.93 (s, 1H), 5.25 (s, 1H), 7.01 (t, J = 7.8 Hz, 1H), 7.11 (t, J = 7.8 Hz, 1H), 7.31 (d, J = 7.8 Hz, 1H), 7.55 (d, J = 7.8 Hz, 1H), 8.16 (s, 1H). ^{13}C NMR (100 MHz, $CDCl_3$, δ, ppm): 11.9, 24.6, 33.8, 38.5, 42.3, 46.2, 47.7, 108.7, 111.4, 112.1, 118.5, 119.2, 122.8, 127.1, 133.6, 136.3, 138.7.

Found, %: C, 80.86; H, 7.81; N, 11.19. $C_{17}H_{20}N_2$. Calcd, %: C, 80.91; H, 7.99; N, 11.10.

Uleine (6). A mixture of noruleine (100 mg, 0.39 mmol) was dissolved in 30 mL of acetonitrile. After 15 min at rt, and then the mixture was treated with formaldehyde (0.8 mL, 35% w/w aqueous solution, 7.8 mmol) and $NaCNBH_3$ (48 mg, 0.78 mmol). After stirring at room temperature for 1 h, the reaction mixture was quenched with 10% $NaHCO_3$ (30 mL) and extracted with CH_2Cl_2 (3 × 30 mL), dried over anhydrous $MgSO_4$, and concentrated under pressure to give a residue which was then purified by column chromatography (MeOH– CH_2Cl_2, 10:2) and was evaporated to give the title **6** (91 mg, 88%) as a white amorphous solid, mp 165 °C, R_f 0.5 (EtOAc-*n*-hexane, 1:1). IR spectrum (KBr, ν, cm^{-1}): 3415, 3071, 2926, 2881, 1624, 1611, 1537, 1461, 1098, 1011, 887, 778, 751, 618. ^1H NMR (400 MHz, $CDCl_3$, δ, ppm, J/Hz): 0.86 (t, J = 7.4 Hz, 3H), 1.12–1.16 (m, 2H), 1.63–1.71 (m, 1H), 2.06–2.16 (m, 3H), 2.32 (s, 3H), 2.48–2.55 (m, 1H), 2.64–2.71 (m, 1H), 4.13 (s, 1H), 5.01 (s, 1H), 5.26 (s, 1H), 7.11 (t, J = 7.8 Hz, 1H), 7.18 (t, J = 8.2 Hz, 1H), 7.36 (d, J = 8.2 Hz, 1H), 7.56 (d, J = 7.8 Hz, 1H), 8.25 (s, 1H, NH-indole). ^{13}C NMR (100 MHz, $CDCl_3$, δ, ppm): 11.7, 24.6, 34.7, 39.4, 44.2, 46.1, 46.4, 56.8, 107.1, 107.4, 110.7, 119.3, 120.1, 122.7, 129.2, 135.4, 136.7, 138.7.

Found, %: C, 81.22; H, 8.39; N, 10.46. $C_{18}H_{22}N_2$. Calcd, %: C, 81.16; H, 8.32; N, 10.52.

2.3. DFT and TD-DFT calculations

The compounds **3–6** (Scheme 1) were optimized B3LYP [60, 61]/6-311G(d,p) [62, 63, 64] level of theory in both the gas and chloroform phases. PCM "polarized continuum model" [65, 66, 67] was used to simulate the chloroform (ε = 4.71) media at the same level of theory. In all computations, the default convergence criteria for both geometry optimization (ref) by Berny algorithm using GEDIIS [68] and SCF procedure with no damping or Fermi broadening [69] have been applied. All optimized structures were confirmed by the absence of the imaginary frequency. All DFT computations and analyses of the results were utilized by using the packages of G09 [70] and GaussView 6.0.16 [71].

The thermodynamic quantities and physical properties of the compounds were investigated considering the quantum mechanics [72, 73]. Accordingly, the total partition function of a specific system, based on the freedom degrees of translational, rotational, vibrational, and electronic, is defined as below:

$$Q = Q_{trans.}\ x\ Q_{rot.}\ x\ Q_{vib.}\ \ Q_{elec.}$$

For the asymmetric top molecules, the vibrational partition function depending on the normal modes is calculated by the following equation [74, 75]:

$$Q_{vib.} = \prod_{j=1}^{3N-6} \frac{e^{-\Theta_{v,j}/2T}}{\left(1 - e^{-\frac{\Theta v,j}{T}}\right)}$$

Then, the vibrational part of the thermodynamic quantities $E_{vib.}$ "vibrational thermal energy", $S_{vib.}$ "vibrational entropy", and $Cv_{vib.}$ "vibrational heat capacity" is defined as [72, 73, 74, 75].

$$E_{vib.} = Nk \sum_{j=1}^{3N-6} \left(\frac{\Theta_{v,j}}{2} + \frac{\Theta_{vj}\, e^{-\Theta_{v,j}/T}}{\left(1 - e^{-\frac{\Theta v,j}{T}}\right)} \right)$$

$$S_{vib} = Nk \sum_{j=1}^{3N-6} \left[\frac{\Theta_{v,j}/T}{\left(e^{\Theta_{v,j}/T} - 1\right)} - ln\left(1 - e^{-\Theta_{v,j}/T}\right) \right]$$

$$Cv_{vib.} = Nk \sum_{j=1}^{3N-6} \left[\left(\frac{\Theta_{vj}}{T}\right)^2 \frac{e^{\Theta_{vj/T}}}{\left(e^{\Theta_{v,j}/T} - 1\right)^2} \right]$$

The terms are expressed as $\Theta_{vj} = \frac{h\nu_j}{k}$ "the vibrational temperature", h→ "Planck constant", k→ "Boltzmann constant", and ν_j→" jth fundamental frequency".

In addition, the chemical reactivity properties were evaluated in light of the conceptual DFT. Accordingly, the values I "ionization energy" and A "electron affinity" [76] are determined, and then these values are used for calculating further reactivity parameters as follows;

$$I = -E_{HOMO}$$

$$A = -E_{LUMO}$$

$$\chi = -\left(\frac{I + A}{2}\right)$$

$$\eta = \frac{I - A}{2}$$

$$\omega = \frac{\mu^2}{2\eta}$$

$$\Delta N_{max} = \frac{I + A}{2(I - A)}$$

$$\omega^{+} \approx (I + 3A)^2 \Big/ 16((I - A))$$

$$\omega^{-} \approx (3I + A)^2 \Big/ 16((I - A))$$

$$\Delta\varepsilon_{back-donation} = -\frac{\eta}{4}$$

Terms are defined as χ → "electronic chemical potential" η → "global hardness", ω → "electrophilicity", ΔN_{max} → "the maximum charge transfer capability index" [77, 78, 79, 80, 81, 82], ω- "the electro-donating power" and ω+ "the electroaccepting power" [83], and $\Delta E_{back\text{-}donat.}$ "back-donation energy" [84].

Last, the possible electronic transitions that contributed to the lowering stabilization energy ($E^{(2)}$) were determined by performing NBO [85, 86, 87, 88] analyses. For a specific molecule, the value of $E^{(2}$ is a function of *qi* → "the donor orbital occupancy"; *εi* and *εj* → "donor and acceptor orbital energies (diagonal elements)"; *Fij* → "the off-diagonal NBO Fock matrix element" and is defined as

$$E^{(2)} = \Delta E_{ij} = qi\frac{(Fij)^2}{(\varepsilon j - \varepsilon i)}$$

The NMR shifts of compounds **3–6** were calculated by using GIAO "Gauge-Independent Atomic Orbital" [89, 90] approach to the shift constant of TMS (tetramethylsilane), in CHCl3. Last, molecular properties [91], bioactivity parameters [91], and drug-likeness model scores [92] of compounds **3–6** were explored by using online tools.

2.4. Molecular docking methods

The molecular docking procedures were performed with AutoDock 4.2 against AChE, BuChE, and HSA crystal structures. All the structures were downloaded from RCSB protein data bank (https://www.rcsb.org/) (PDB ID: 3lii for AChE, 1p0i for BuChE, and 1bm0 for HSA) [93, 94, 95]. The maximum torsion number with fewest atom was set for the ligand molecules. Kollman charges were regarded, and only polar hydrogens were employed in all target crystal structures [96]. Water molecules in the targets were extracted and also Gasteiger charges, and Randomized starting positions were utilized during the processes. Lamarckian genetic algorithms were employed with 150 genetic algorithm populations for 10 runs [97, 98]. The grids in 0.375 spacing were selected as 40/40/40 npts with 29.607/31.782/23.488 (x/y/z) in 1bm0; 90/68/70 npts with 139.891/117.013/45.220 (x/y/z) in 1p0i; and 56/50/74 npts with 94.160/87.917/-4.492 (x/y/z) in 3lii for all ulein type molecules. The standart program defaults were used during the running. All the illustrations were performed with Discovery Studio 4.1.0.

3. Result and discussion

3.1. Synthesis and spectroscopic characterization

In this work, the effectiveness of this route has been demonstrated by the efficient short synthesis of **(±)**-noruleine and **(±)**-uleine. This methodology was extended to other alkaloids and the broad family of natural products. This system is the first example of a one-pot construction of the tetracyclic 12-ethyl-1,2,3,4,5,6-hexahydro-1,5-methanoazocino [4,3-b]indole-3,6-dione (**3**) using TFB starting with 2-(3-ethyl-1-oxo-2,3,4,9-tetrahydro-1H-carbazol-2-yl)acetonitrile **1**. Further, the work could be applied in a novel approach to the synthesis of *strychnos* alkaloids. The measured FT-IR and NMR spectra of the reagents and products (compounds **2–6**) were given in Figures S1, S2, S3, S4, S5 (suppl.data). .

The selected functional vibrations for compounds **3–6** were presented in Table 1. The observed peaks at 3241 (**3** and **5**), 3254 (**2**), and 3415 cm^{-1} (**6**) were associated with the N–H elongation mode assigned at 3443 (**3**), 3442 (**4**), 3376 (**5**), and 3533 cm-1 (**6**), respectively. Recently, the vN-H bond vibration was observed at 3232, 3230, 3426 and assigned at 3543, 3523, 3447 cm-1 [31, 44, 45], respectively. Very strong peaks appeared at 1664 and 1654 cm-1 were markers of the carbonyl group (C=O) in compounds **3** and **4** and computed at 1704 and 1702 cm^{-1}. Recently, the C=O vibrational mode for thiophene derivatives that were structurally similar molecules was observed at 1674, 1664, and 1663 cm^{-1} and calculated by B3LYP/6–311++G(d,p) level at 1731 and 1730 cm^{-1} [99]. The νN = C elongation mode for compound **3** appeared at 1429 cm^{-1} and was calculated at 1431 cm^{-1}. On the other hand, the νN = C elongation mode for compound **4** was calculated at 1468, 1428, 1419, 1413, and 1296 cm^{-1} accompanied by the ipb(HNC + HCC) bending modes generally. For compounds 5 and 6, the νN = C vibrations were computed in the range of 1466–1215 cm^{-1} and 1466-1297 cm^{-1}, the peaks calculated at 1466 for both compounds were very strong and mixed with ipbHNC mode. For compounds **4–6**, the measured peaks at 1621, 1671, and 1624 cm^{-1} were estimated at 1619, 1616, and 1615 cm^{-1}, respectively. On the other hand, the observed peaks at 1530, 1580, 1574, and 1537 cm^{-1} were associated with the C–C bond stretching for the aromatic rings predicted at 1520, 1591, 1590, and 1551 cm^{-1}, and were contaminated with the ipbHCC bending modes. Here, the scaling factor 0.9619 [100] for the B3LYP/6-311G(d,p) level of theory was used to compatible the calculated vibrations with the measured data.

The observed and computed NMR shifts for compounds **3–6** were given in Tables 2 and 3. For compounds **3–6**, the proton shift for the indole ring was measured at 9.51, 11.23, 8.16, and 8.35 ppm, calculated at 8.16, 7.81, and 7.88 pm. For compound **3**, the aromatic proton shifts (H30–H33) were observed in 7.73–7.35 ppm and calculated in 8.02–7.47 ppm. The counterpart carbon shifts for the compounds were observed in the range of ~140-100 ppm. The ^{13}C NMR shifts for the unsaturated carbon atoms of compounds **3–6** were observed in the range of 138.5–112.3, 135.4–109.2, 136.3–108.7, and 136.7–107.1 ppm, whereas they were assigned in 144.1–117.4, 143.0–110.3, 143.4–108.6, 142.9–108.7 ppm, respectively. As known well from previous reports, C and H atoms exhibit a higher chemical shift with the magnetic resonance beam, according to the electronegativity of the groups around a related atom. Here, the chemical shifts related to the carbon atoms (C8 and C9) for compounds **3** were recorded at 172.2 and 191.4 ppm and determined at 174.2 and 197.0 ppm because of the existence of the oxygen atom. From Tables 2, 3, the regression coefficients for compounds **3–6** revealed that the observed data are compatible with both the calculated and reported data, R^2 values for both ^1H and ^{13}C NMR shifts were calculated in 0.929–0.963 and 0.997–0.999, respectively.

3.2. Molecule geometry and physicochemical properties

The optimized structures and geometric parameters of compounds **3–6** were presented in Figure 1 and Table 4, respectively. Accordingly, the bond length N1–C4 was reported as 1.48 Å [101] and predicted as 1.49 Å for noruleine (**5**) and uleine (**6**). The bond lengths N2–C11 and N2–C13 were determined as 1.38 Å and 1.37 Å for compound **3**, reported as 1.37 Å [102] for structurally related compounds. besides, the C18–C19 bond on the aromatic ring was reported as 1.39 Å [101, 102] and calculated for compounds **3–6** as 1.41 Å. On the other hand, the bond angle C16–C18–C19 was observed at 121.7° [101] and calculated at 121.0–121.1° for compounds **4–6**. As expected from sp^3 hybridization, the angles N1–C4–C3, N1–C4–C7, N2–C11–C7, C11–N2–C13, and C4–C3–C5 were observed at 109.2°, 112.3°, 110.5°, 108.5°, and 107.7°, respectively, where the same angles for uleine were calculated as 107.7, 114.4, 109.2, 109.3, and 107.0 Å. For compounds **3** and **4**, the C8–N1–C4

Table 1. The observed and calculated vibrational frequencies (in cm^{-1}) of the compounds at B3LYP/6-311G(d,p) level.

	3		4		5		6	
Assignment	*Exp.*	*Scal.*	*Exp.*	*Scal.*	*Exp.*	*Scal.*	*Exp.*	*Scal.*
νNH	3241	3443	3254	3442	3241	3376	3415	3533
ν_{as}*CH2*	—	—		3092		3088		3088
νCH(ar.)	3073	3071		3067		3066	3071	3067
νCH(ar.)		3061	3051	3056		3054		3057
νCH(ar.)		3050		3045		3044		3046
νCH(ar.)		3044		3040		3038		3039
ν*CH2*		—		3016		3013		3013
ν_{as}CH2		2975		2974		2972		2972
ν_{as}CH2		2971	2966	2970	2963	2966		2966
νCH	2961	2954		2951	2922	2951		2951
νCH		2946		2944		2942		2941
ν_{as}CH2		2941		2929		2938	2926	2928
νCH2	2917	2923		2915		2937		2921
νCH3		2910	2913	2908		2907		2906
νCH2	2850	2907	2887	2904		2905		2905
νCH		2898	2881	2899		2904		2904
νC = O	1664	1704	1654	1702	—	—	—	—
νC = O	1611	1670	—	—	—	—	—	—
ν*(R–C=CH2)*	—	—	1621	1619	1619	1616	1611	1615
νCC + ipb HNC	1578	1596	1580	1591	1574	1590		1589
νCC + ipb HNC		1548	1544	1552		1551	1537	1551
νCC + ipb HNC+ δ*C* = *C*H2	1530	1520				1505		1507
νCC + ipb HNC		1473	1482	1468		1467	1461	1467
δCH2		1453	1453	1453	1457	1454	1440	1445
δCH2	1429	1435		1434		1433		1433
νNC + ipb HNC		1430	1404	1404		1417		1417
sbCH3		1364	1358	1363		1362		1361
ipb (HNC + HCC)	1351	1352		1353		1355		1349
(ω+ τ) CH2		1344		1344		1342	1330	1337
νNC + ipb HNC+ τ CH2	1325	1329		1330	1329	1335		1327
ipb HNC		1322		1321		1316		1234
ipb HCC+ (ω+ τ) CH2	1242	1253	1251	1255		1258		1219
(ω+ τ) CH2	1236	1236		1241		1239		1216
ipb (HNC + HCC)	1155	1155	1222	1228	1201	1226	1127	1132
τ CH2	1132	1138		1149	1166	1145	1098	1099
ipb (HNC + HCC)+ νCC		1104	1077	1092	1134	1131		1052
β CCC+ νCC	980	992				996		995
(ω+ ρ) CH2		953	975	969		966		983
opb HCC		947	783	774		935		935
opb HNC		760		645	738	749	751	739
opb HNC	618	634		624		612		559

*The abbreviation are ν, symmetric stretching; $\nu_{as,}$ asymmetric stretching; ω, wagging; τ, twisting; ρ, rocking; δ, scissoring; β, bending; ipb, in-plane bending; opb, out-plane bending.

was calculated at 124.2° and 123.4° due to the effect of electron delocalization of the neighbor –C=O group on this bond. On the other hand, the same angle of noruleine (**5**) and uleine (**6**) was calculated at 113.1°, and 112.8° as expected from typical sp^3 hybridization. For compounds **3** and **4**, the angle N1–C8–O38 was predicted as 121.9° and 122.2° and was reported as 122.3° [102]. Furthermore, the angle C11–N2–C13 for compounds **5** and **6** was determined as 109. 3° and recorded [102] as 108.5° in past. From Table 4, the dihedral angles N1–C4–C3–C5, N1–C4–C7–C11, and N1–C8–C6–C5 for uleine (**6**) were determined as 66.0°, -89.3°, and -49.9°, whereas these angles for noruleine (**5**) were calculated as 65.7°, -89.1°, -50.9°. Furthermore, N2–C11–C9–C5, N2–C11–C9–C15, and N2–C11–C7–C4 angles were found to be -178.9°, 1.3°, and 179.9° for **6**, whereas they were calculated for compound **5** as -176.2°, 3.7°, and 178.3°. There are some small deviations from the reported values of the calculated data because the experimental data of the structurally related azocino-indole [101, 102] compounds were used for comparison purposes.

In addition Table 5 summarized the calculated thermodynamic quantities and physical parameters of compounds **3–6**. With increasing the dielectric constant of the simulation media, even not much great, thermodynamic quantities for all compounds decreased. Namely, the electronic energies (ΔE), enthalpy (ΔH), and free energy (ΔG) changing for **6** were calculated in the gas phase as -808.496919, -808.478746, and -808.540646 au, whereas they were determined in $CHCl_3$ as -808.502446, -808.484293, and -808.546208 au, respectively. Besides, the $E_{therm.}$, Cv, and S values of compound **6** were determined in $CHCl_3$ as 239.011 kcal/mol, 71.020 cal/mol K, 130.310 cal/mol K, and 130.310 cal/mol K contributed by the vibrational motion freedom by 237.234 kcal/mol, 65.058 cal/mol K, and 54.298 cal/mol K. Especially, the contribution of the vibrational freedom to total quantities is remarkable

Table 2. The observed and calculated 13C NMR chemical shifts of the studied compounds relative to TMS, at B3LYP/6-311G(d,p) level of the theory in CHCl3.

3			4			5			6		
Atom	Exp.	Calc.	Atom	Exp.	Calc.	Atom	Exp.	Calc.	Atom	Exp.	Calc.
3-C	45.3	54.3	3-C	41.5	50.6	3-C	47.7	53.6	3-C	46.4	54.5
4-C	44.1	51.5	4-C	44.9	51.4	4-C	46.2	53.3	4-C	56.8	59.7
5-C	47.9	56.2	5-C	43.6	50.9	5-C	42.3	51.4	5-C	46.1	50.4
6-C	35.6	42.2	6-C	38.8	47.1	6-C	33.8	41.4	6-C	34.7	41.4
7-C	128.8	135.7	7-C	118.1	123.8	7-C	112.1	118.8	7-C	110.7	115.4
8-C	172.2	174.2	8-C	172.2	176.2	8-C	38.5	42.6	8-C	44.2	50.3
9-C	191.4	197.0	9-C	139.1	150.2	9-C	138.7	150.4	9-C	138.7	150.3
10-C	23.5	29.5	10-C	22.6	29.4	10-C	24.6	30.1	10-C	24.6	29.7
11-C	128.3	134.9	11-C	130.3	138.0	11-C	133.6	141.5	11-C	135.4	141.7
12-C	124.6	131.9	12-C	123.7	132.7	12-C	127.1	133.5	12-C	129.2	136.1
13-C	138.5	144.1	13-C	135.4	143.0	13-C	136.3	143.4	13-C	136.7	142.9
14-C	11.3	14.1	14-C	11.4	14.2	14-C	11.9	14.0	14-C	11.7	14.0
15-C	121.2	126.7	15-C	109.2	110.3	15-C	108.7	108.6	15-C	107.1	108.7
16-C	112.3	117.4	16-C	117.7	123.6	16-C	118.5	124.0	16-C	120.1	125.3
17-C	121.8	127.1	17-C	112.5	115.5	17-C	111.4	115.1	17-C	107.4	114.9
18-C	127.4	133.8	18-C	118.9	125.8	18-C	119.2	125.1	18-C	119.3	125.0
			19-C	121.7	129.5	19-C	122.8	128.7	19-C	122.7	128.6
									38-C	39.4	46.4
R2 = 0.999			R2 = 0.997			R2 = 0.997			R2 = 0.998		

Table 3. The observed and calculated ^{1}H NMR chemical shifts of the studied compounds relative to TMS, at B3LYP/6-311G(d,p) level of the theory in $CHCl_3$.

3			4			5			6		
Atom	Exp.	Calc.	Atom	Exp.	Calc.	Atom	Exp.	Calc.	Atom	Exp.	Calc.
19-H	2,49	2,62	20-H	2,19	2,37	20-H	2,08	2,03	20-H	2,11	2,04
20-H	4,75	4,86	21-H	4,33	4,68	21-H	4,34	4,43	21-H	4,13	4,14
21-H	2,96	2,64	22-H	2,83	2,78	22-H	2,60	2,45	22-H	2,52	2,41
22-H	2,96	2,89	23-H	2,93	2,88	23-H	2,08	2,05	23-H	2,32	2,12
23-H	2,49	2,31	24-H	2,05	2,16	24-H	2,08	1,55	24-H	1,67	1,62
24-H	1,38	1,30	25-H	1,15	1,21	25-H	1,26	1,15	25-H	1,14	1,10
25-H	1,38	1,57	26-H	1,15	1,46	26-H	1,63	1,21	26-H	1,14	1,20
26-H	9,51	8,16	27-H	11,23	7,81	27-H	8,16	7,81	27-H	8,25	7,88
27-H	0,96	1,01	28-H	0,88	1,01	28-H	1,26	1,04	28-H	0,86	1,04
28-H	0,96	0,94	29-H	0,88	0,93	29-H	0,79	0,85	29-H	0,86	0,85
29-H	0,96	1,06	30-H	0,88	1,03	30-H	0,79	0,94	30-H	0,86	0,93
30-H	7,73	8,02	31-H	5,01	5,18	31-H	4,93	5,04	31-H	5,01	5,05
31-H	7,37	7,63	32-H	5,57	5,46	32-H	5,25	5,42	32-H	5,26	5,42
32-H	7,35	7,47	33-H	8,22	7,79	33-H	7,55	7,75	33-H	7,56	7,79
33-H	7,47	7,66	34-H	7,54	7,49	34-H	7,31	7,49	34-H	7,36	7,47
34-H	7,15	5,34	35-H	7,18	7,34	35-H	7,01	7,29	35-H	7,11	7,27
			36-H	7,36	7,45	36-H	7,11	7,40	36-H	7,18	7,39
			37-H	7,06	5,22	37-H	0,79	0,87	37-H	2,32	2,29
						38-H	2,60	2,58	39-H	2,11	2,01
						39-H	2,60	2,64	40-H	2,32	2,21
									41-H	2,68	2,62
									42-H	2,11	2,02
R^2 = 0.963			R^2 = 0.929			R^2 = 0.994			R^2 = 0.997		

as expected. For reagent **4**, the thermodynamic state functions S, $S_{tr.}$, $S_{rot.}$, and $S_{vib.}$ (in cal/mol K) were calculated as 129.016, 42.636, 33.488, and 52.893, respectively. The ordering of the dipole moment μ (D) was changed as 4.648 (**3**) > 4.264 (**4**) > 1.767 (5) > 1.623 (**6**) in the gas and 5.749 (**3**) > 5.237 (**4**) > 2.317 (**5**) > 2.188 (**6**) in $CHCl_3$. Furthermore, the polarizability values α (au) changed in the order of 191.774 (**3**) < 204.477 (**4**) < 204.384 (**5**) < 216.223 (**6**) in the gas phase and as 240.414 **(3) <** 257.498 **(4) <** 258.785 **(5) <** 274.042 (**6**) in $CHCl_3$**.** Both dipole moment and polarizability were affected by the chloroform dielectric simulation media. Also, reagents **3** and **4** have greater dipole moments than those of the noruleine and uleine, because of the existence of additional electronegative oxygen atoms.

3.3. NBO analysis

NBO method [85, 86, 87, 88] has been used for evaluating the non-covalent interactions such as anomeric, hyperconjugative, and cieplak as well as the resonances, and is increasingly applied to organic [23,

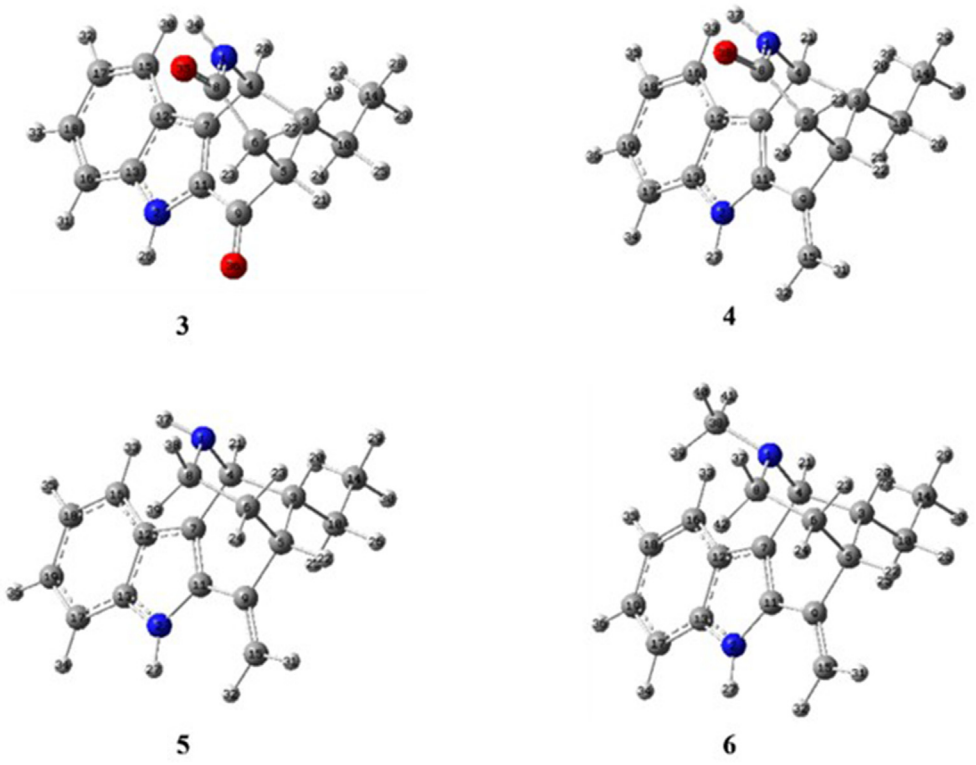

Figure 1. The optimized structures of the compounds **3–6** in the gas phase.

29, 45] and inorganic [103, 104] systems. We have summarized the possible resonance interactions in Table 6; full details of NBO computations were given in Table S1 (suppl. data).

As can be expected, the main contributions are due to the resonance interactions, the electron moving to antibonding orbital Π* from the lone pair of the nitrogen is remarkable. Namely, the energy of the resonance interaction LP (1) N2→ Π* C7–C11 for compounds **3–6** was determined as 36.84, 36.81, 35.80, and 36.20 kcal/mol, respectively. In addition, the energy of the interaction LP (2) N1→ Π* C12–C13 for compounds **3–6** was determined as 39.29, 31.88, 35.97, and 36.11 kcal/mol and fairly attractive. Also, the other n→ Π* interaction for reagent **3** was determined as LP (1) N1 (ED_i = 1.73079e) → Π* C8–O35 (ED_j = 0.20345e) with the energy of 24.91 kcal/mol (Table S1). Similarly, the energy of the resonance LP (1) N1 (ED_i = 1.73079e) → Π* C8–O38 (ED_j = 0.20345e) for reagent **4** was determined as 23.98 kcal/mol. However, the contribution of this interaction (LP (1) N1→ Π* C8–O38) to $E^{(2)}$ for compounds **5** and **6** was calculated with the energy of 1.32 and 1.21 kcal/mol, respectively. Also, the interactions Π C7–C11 (ED_i = 1.75093e) → Π* C9–O36 (ED_j = 0.18019e) and Π C7–C11 (ED_i = 1.75093e)→ Π* C12–C13 (ED_j = 0.49861e) for reagent **3** were calculated with the energy of 22.87 and 16.40 kcal/mol. Instead of the interaction Π C7–C11→ Π* C9–O36, the resonance Π C7–C11→ Π* C9–C15 for the compounds **4**, **5**, and **6** were determined with the energy of 16.64 16.79, and 16.83 kcal/mol, respectively. In addition, the energies of the resonance interactions for charge transfer to each Π* C7–C11, Π* C15–C17, and Π* C16–C18 from bonding orbital Π C12–C13 for reagent **3** were calculated as 21.62, 19.28, and 18.53 kcal/mol, respectively. For the compound **6**, the counterpart resonance interactions were determined as Π C12–C13→ Π* C7–C11 ($E^{(2)}$ = 19.29 kcal/mol), Π C12–C13→ Π* C16–C18 ($E^{(2)}$ = 19.29 kcal/mol), and Π C12–C13→ Π* C17–C19 ($E^{(2)}$ = 18.75 kcal/mol). All these interactions are responsible for the charge distribution on the compounds and thus the chemical reactivity of the compounds.

3.4. FMO (Frontier Molecular orbital) analysis and MEP (Molecular electrostatic potential)

The global reactivity parameters obtained from quantum chemical computations have been applied to different types of systems for a long time [31, 44, 45, 46, 98, 99, 105, 106, 107]. In this work, The calculated reactivity parameters of the compounds were given in Table 7.

The energy gap (ΔE_{gap}, eV) ordering of the compounds changed as 4.274 (**5**) > 4.265 (**4**) > 4.210 (**6**) > 4.176 (**3**) in the gas and as 4.289 (**5**) ≥ 4.289 (**4**) > 4.234 (**6**) > 4.121 (**3**) in $CHCl_3$. Besides, the hardness η (eV) values were determined as follows 2.137 (**5**) > 2.133 (**4**) > 2.105 (**6**) > 2.088 (**3**) in gas and 2.145 (**5**) ≥ 2.145 (**4**) > 2.117 (**6**) > 2.061 (**3**) in $CHCl_3$. Accordingly, compound **5** and then **4** was determined as the hardest molecules and reagent **3** was the softer. Besides, the energy values implied that these compounds (**5** and **4**) could have gained stability via back donation: the calculated back donation energies of the compounds were determined as:

$\Delta\varepsilon_{back\text{-}donat.}$ (eV): -0.534 (**5**) ≥ -0.533 (**4**) > -0.526 (**6**) > -0.522 (**3**) in the gas

$\Delta\varepsilon_{back\text{-}donat.}$ (eV): -0.536 (**5**) ≥ -0.536 (**4**) > -0.529 (**6**) > -0.515 (**3**) in $CHCl_3$.

Also, the χ (eV) values was calculated in the following order: -4.143 (**3**) < -3.558 (**4**) > -3.304 (**5**) > -3.274 (**6**) in the gas and -4.102 (**3**) < -3.514 (**4**) > -3.350 (**5**) > -3.332 (**6**) in $CHCl_3$. Related to the electrophilicity indexes, the order of ω (eV) was determined as **3** (0.151) > **4** (0.109) > **5** (0.094) ≥ **6** (0.094) in the gas phase and with the same order in $CHCl_3$: reagent **3** has the highest electrophilicity value and vice versa for the uleine (**6**). Also, the electrodonating and electroaccepting indexes in the gas phase were calculated in the following orders:

ω^{+} *(au)*: **3** (0.085) > **4** (0.053) > **5** (0.043) ≥ **6** (0.043)

Table 4. The selected optimized parameters for the synthesized compound **3–6** at B3LYP/6-311G(d,p) basis set in the gas.

Bond Length (Å)	*Exp.*[*]	3	4	5	6
N1–C4	1.48[a]	1.48	1.48	1.49	1.49
N1–C8	1.34[b]	1.38	1.37	1.47	1.46
N1–C38	1.47[a]	—	—	—	1.46
N2–C11	1.37[b]	1.38	1.39	1.39	1.39
N2–C13	1.37[b]	1.37	1.38	1.39	1.38
C8–O35	1.24[a]	1.22	1.22	—	—
C8–O38	—	—	—	—	—
C9–O36	—	1.22	—	—	—
C3–C10	1.51[a]	1.54	1.54	1.54	1.54
C5–C6	1.53[b]	1.55	1.55	1.55	1.55
C9–C15	—	—	1.34	1.34	1.34
C18–C19	1.39[a,b]	—	1.41	1.41	1.41
R^2		*0.9758*	*0.9815*	*0.7059*	*0.7137*
Bond angle (°)					
N1–C4–C3	109.2[a]	108.0	108.0	107.3	107.7
N1–C4–C7	112.3[a]	111.4	111.7	113.8	114.4
N1–C8–O38	122.3[b]	121.9	122.2	—	—
C8–N1–C4	121.0[b]	124.2	123.4	113.1	112.8
C8–N1–C38	120.6[a]	—	—	—	111.7
N2–C11–C9	—	125.3	126.9	126.7	126.4
N2–C11–C7	110.5[a]	110.0	110.0	109.2	109.2
C11–N2–C13	108.5[b]	108.8	109.3	109.3	109.3
C4–C3–C5	107.7[a]	106.9	106.6	106.9	107.0
C3–C10–C14	—	114.4	114.4	114.3	114.3
C5–C6–C8	118.9[a]	116.5	117.2	112.7	112.8
C5–C9–C15	—	—	121.7	121.9	121.8
C11–C9–C15	—	—	124.3	124.2	124.2
C16–C18–C19	121.7[a]	—	121.1	121.0	121.1
C11–C9–O36	—	123.0	—	—	—
R^2		*0.945*	*0.967*	*0.684*	*0.548*
Dihedral angle (°)					
N1–C4–C3–C5	65.4[b]	62.7	64.1	65.7	66.0
N1–C4–C7–C11	89.0[a]	-86.7	-88.5	-89.1	-89.3
N1–C8–C6–C5	3.7[b]	-18.5	-18.9	-50.9	-49.9
C8–N1–C4–C3	-40.5[a]	-43.3	-45.4	-64.5	-63.4
C8–N1–C4–C7	80.0[a]	77.2	75.2	56.2	57.7
C4–N1–C8–O35	-176.6[b]	-163.6	—	—	—
C4–N1–C8–O38	—	—	-162.3	—	—
N2–C11–C9–O36	—	-0.5	—	—	—
N2–C11–C9–C5	-175.3[a]	-179.0	-176.6	-176.2	-178.9
N2–C11–C9–C15	—	—	3.5	3.7	1.3
N2–C11–C7–C4	179.2[b]	177.7	178.2	178.3	179.9
C11–N2–C13–C12	-0.4[a]	-0.0	0.5	0.6	0.2
C4–C3–C5–C9	68.7[b]	59.8	62.0	62.9	62.6
C4–C3–C10–C14		62.0	63.1	63.6	63.5
C16–C18–C19–C17	−0.8[b]	—	-0.1	-0.1	-0.3
R^2		*0.777*	*0.705*	*0.710*	*0.7134*
R^2		*0.8465*	*0.8114*	*0.7949*	*0.8045*

[*] Available experimental data were taken from Refs. a [101] and b [102].

ω^- *(au)*: **3** (0.237) > **4** (0.184) > **5** (0.164) > **6** (0.163)

Here, the electrodonating power of all compounds was greater 3 times than the electroaccepting potency and the same order was determined in $CHCl_3$ simulation media. Due to the lone pair of the oxygen atom, compound **3** has the greatest electro-donating power more than the other compounds.

In addition, the possible reactivity sites for the nucleophilic and electrophilic attacks of the compounds **3–6** were illustrated in Figure 2. For reagents **3** and **4**, the HOMO expanded on the indole ring and –C=O group, partially on the aliphatic ring, whereas the LUMO broadened on the indole and slightly saturated ring. For compounds **5** and **6**, HOMO enlarged on the indole and = CH2 group on the saturated ring, on N1 atom around a little. Also, the MEP plots for reagents **3** and **4** indicated that the –C=O group was an essential role in electrophilic attacks due to bearing the red color ($V < 0$) that was a marker of the electron-rich region. But for compounds **5** and **6**, the indole ring was covered orange color that showed a moderate size electron-rich region. For all compounds, the hydrogen of –NH group on the indole ring would be important for the nucleophilic attacks since it was covered by blue color ($V > 0$).

3.5. Molecular docking analysis

Acetylcholinesterase inhibitors are frequently used in the treatment of AD. Tacrine whose IC_{50} value is 205 nM, is the first-approved AChE inhibitor for the treatment of cognitive symptoms of AD in 1993. Hepatotoxicity profile and dosage frequency are common limitations of tacrine [108]. The IC_{50} values of Donepezil, Rivastigmine, and Galantamine, which were approved by the FDA in the following years, were determined as 11.6 nM, ~4.3nM, and 410 nM, respectively [109, 110, 111]. Molecular docking methods have also been frequently used for the detailed analysis of the interaction mechanisms of these drugs with various biomacromolecules. Burmaoglu et al. analyzed the AChE inhibition potential of biphenyl-substituted chalcone derivative molecules, and they determined that the tacrine formed H-bonds with Trp84 and Tyr334 [112]. Ahmed et al. performed their study for 1, 3-di-4-piperidylpropane derivatives molecules. They noted that donepezil and galantamine interacted with approximately the same region of AChE, donepezil made H-bonds with Phe295, and galantamine interacted with H-bonds with Gly122 [113]. Islam et al. examined the AChE inhibition of Donepezil, Galantamine, Rivastigmine and Tacrine theoretically, determined the binding affinities as -7.9, -8.0, -8.6, and -8.6 kcal/mol, respectively, and emphasized H-bonds of these molecules with Tyr124 and Ser293 [114]. In another study, Çelik et al investigated the enzyme inhibition properties of 2,5-Disubstituted Benzoxazole derivatives and the binding energy of Galantamine was calculated as −9.4 kcal/mol with Vina [115]. Uleine, which is a natural alkaloid extracted from Himatanthus lancifolius, has 0.45μM of IC_{50} [12] and the substitution of uleine-derivative molecules differences the activity remarkably [108]. Therefore, in this study, AChE and BuChE inhibition activities of the molecules were analyzed by using molecular docking methods and compared with the results obtained for tacrine and galantamine.

According to the results of this study, the strongest interaction with AChE was detected for **6** with a binding affinity of -8.66 kcal/mol, and four H-bonds with Gly120, Tyr133, Tyr337, and Trp66 were detected between the molecule and the enzyme. Also, π-interaction with His447, alkyl interaction with Gly121, and many van der Waals interactions contributed to the binding affinity. The binding affinities of **3**, **4**, and **5** were recorded as -8.27, -8.46, and -8.52 kcal/mol, respectively. All of the molecules interacted with the same region of the enzyme and this zone was very close to where tacrine and galantamine interacted (Figure 3). All of the studied molecules had higher binding affinity than both drug molecules. The interactions of molecules with BuChE were also analyzed by molecular docking methods in this study. It was calculated the highest binding affinity with -8.29 kcal/mol for **4**. Three H-bonds were detected with BuChE by Trp82, Trp430, and Tyr440. H-bonds, π-, alkylic, and many van der Waal interactions were detected for all molecules. Owing to these interactions, the binding affinities for **3**, **5**, and **6** molecules were calculated as -7.89, -8.04, and -8.15 kcal/mol, respectively (Figure S6). Uleine derivatives, tacrine, and galantamine interacted with approximately the same site of BuChE, and binding affinities were calculated as -6.44 kcal/mol for tacrine and -7.10 kcal/mol for galantamine (Table 8).

Table 5. The thermodynamic and physical values of compounds **3-6**.

		3	4	5	6
Gas (ε = 0.0)	ΔE (au)	-879.253547	-843.288411	-769.207140	-808.496919
	ΔH (au)	-879.236457	-843.270898	-769.190439	-808.478746
	ΔG (au)	-879.297073	-843.332279	-769.249409	-808.540646
	$E_{therm.}$ (kcal/mol)	195.098	209.749	221.136	239.161
	$E_{vib.}$ (kcal/mol)	193.321	207.971	219.359	237.384
	Cv (cal/mol K)	65.297	67.673	65.640	71.048
	$Cv_{vib.}$ (cal/mol K)	59.335	61.711	59.679	65.086
	S (cal/mol K)	127.577	129.187	124.114	130.279
	$S_{tr.}$ (cal/mol K)	42.658	42.636	42.475	42.636
	$S_{rot.}$ (cal/mol K)	33.479	33.480	33.109	33.374
	$S_{vib.}$ (cal/mol K)	51.439	53.071	48.529	54.269
	μ (D)	4.648	4.264	1.767	1.623
	α (au)	191.774	204.477	204.384	216.223
$CHCl_3$ (ε = 4.71)	ΔE (au)	-879.265650	-843.299189	-769.213248	-808.502446
	ΔH (au)	-879.248550	-843.281722	-769.196585	-808.484293
	ΔG (au)	-879.309201	-843.343021	-769.255467	-808.546208
	$E_{therm.}$ (kcal/mol)	195.008	209.702	221.016	239.011
	$E_{vib.}$ (kcal/mol)	193.231	207.925	219.239	237.234
	Cv (cal/mol K)	65.326	67.578	65.587	71.020
	$Cv_{vib.}$ (cal/mol K)	59.364	61.616	59.625	65.058
	S (cal/mol K)	127.649	129.016	123.927	130.310
	$S_{tr.}$ (cal/mol K)	42.658	42.636	42.475	42.636
	$S_{rot.}$ (cal/mol K)	33.485	33.488	33.112	33.376
	$S_{vib.}$ (cal/mol K)	51.506	52.893	48.341	54.298
	μ (D)	5.749	5.237	2.317	2.188
	α (au)	240.414	257.498	258.785	274.042

"The abbreviations are E_{therm}, thermal energy (in kcal/mol); Cv, heat capacity (in cal/mol K); S, entropy (in cal/mol K); μ, dipole moment (in D); α, polarizability (in au); $E_{vib.}$, $Cv_{vib.}$, and $S_{vib.}$ shows the vibrational contribution to the total thermal energy, total heat capacity, and absolute entropy".

Table 6. The stabilization energy lowering (in kcal/mol) of compounds **3–6**, at B3LYP/6-311G(d,p) in gas.

Donor(i)	*Acceptor (j)*	3	4	5	6
Π C7–C11	Π* C9–O36	22.87	—	—	—
	Π* C12–C13	16.40			
Π C7–C11	Π* C9–C15	—	16.64	16.79	16.83
	Π* C12–C13		17.13	17.24	17.27
Π C9–C15	Π* C7–C11	—	13.15	12.88	12.97
Π C12–C13	Π* C7–C11	21.62	—	—	—
	Π* C15–C17	19.28			
	Π* C16–C18	17.09			
Π C12–C13	Π* C7–C11	—	19.64	19.34	19.29
	Π* C16–C18		19.67	19.92	19.86
	Π* C17–C19		18.53	18.81	18.75
Π C15–C17	Π* C12–C13	16.62	—	—	—
	Π* C16–C18	19.65			
Π C16–C18	Π* C12–C13	20.02	17.16	16.99	16.89
	Π* C17–C19	16.96	19.68	19.77	19.82
Π C17–C19	Π* C12–C13	—	19.79	19.58	19.57
	Π* C16–C18		17.43	17.31	17.22
LP (1) N1	Π* C8–O35	24.91	—	—	—
LP (1) N1	Π* C8–O38	—	23.98	1.32	1.21
LP (1) N2	Π* C7–C11	36.84	36.81	35.80	36.20
	Π* C12–C13	39.29	31.88	35.97	36.11

Table 7. The chemical reactivity values of the compounds **3-6**.

		3	4	5	6
Gas	H (-I) (eV)	-6.231	-5.690	-5.441	-5.379
	L (-A) (eV)	-2.055	-1.425	-1.167	-1.169
	ΔE_{gap} (L-H) (eV)	4.176	4.265	4.274	4.210
	χ (eV)	-4.143	-3.558	-3.304	-3.274
	η (eV)	2.088	2.133	2.137	2.105
	ω (eV)	0.151	0.109	0.094	0.094
	ω^+ (au)	0.085	0.053	0.043	0.043
	ω^- (au)	0.237	0.184	0.164	0.163
	ΔN_{max} (eV)	1.984	1.668	1.546	1.555
	$\Delta\varepsilon_{back\text{-}donat.}$ (eV)	-0.522	-0.533	-0.534	-0.526
DMSO	H (-I) (eV)	-6.163	-5.658	-5.495	-5.449
	L (-A) (eV)	-2.041	-1.369	-1.206	-1.215
	ΔE_{gap} (L-H) (eV)	4.121	4.289	4.289	4.234
	χ (eV)	-4.102	-3.514	-3.350	-3.332
	η (eV)	2.061	2.145	2.145	2.117
	ω (eV)	0.150	0.106	0.096	0.096
	ω^+ (au)	0.084	0.051	0.044	0.045
	ω^- (au)	0.235	0.180	0.168	0.167
	ΔN_{max} (eV)	1.990	1.638	1.562	1.574
	$\Delta\varepsilon_{back\text{-}donat.}$ (eV)	-0.515	-0.536	-0.536	-0.529

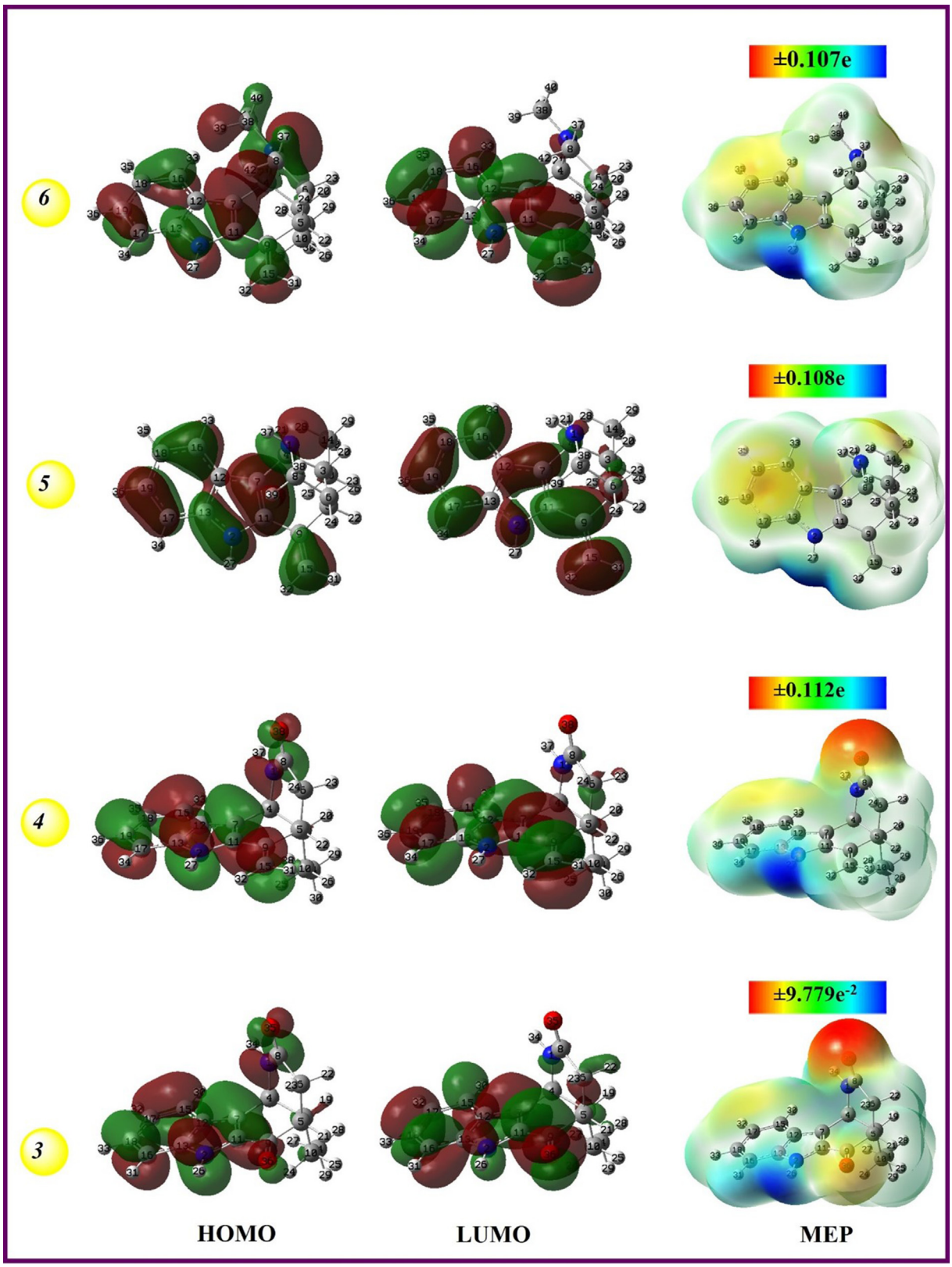

Figure 2. HOMO& LUMO (isoval:0.02), and MEP (isoval:0.0004) plots of the compounds **3–6** at B3LYP/6-311G** level in gas.

Serum albumin which is one of the main components of human blood is responsible for the transport of components such as nitric oxide, oleic and linoleic acids, thyroid and steroid hormones, and vitamin B6 [116]. Serum albumin is also a versatile carrier used for the transport of therapeutic agents used in many diseases such as diabetes and cancer [117]. Therefore, analysis of the interactions with serum albumin is important for the pharmacokinetic evaluation of potentially bioactive molecules. The high binding ability of drug candidate molecules can be

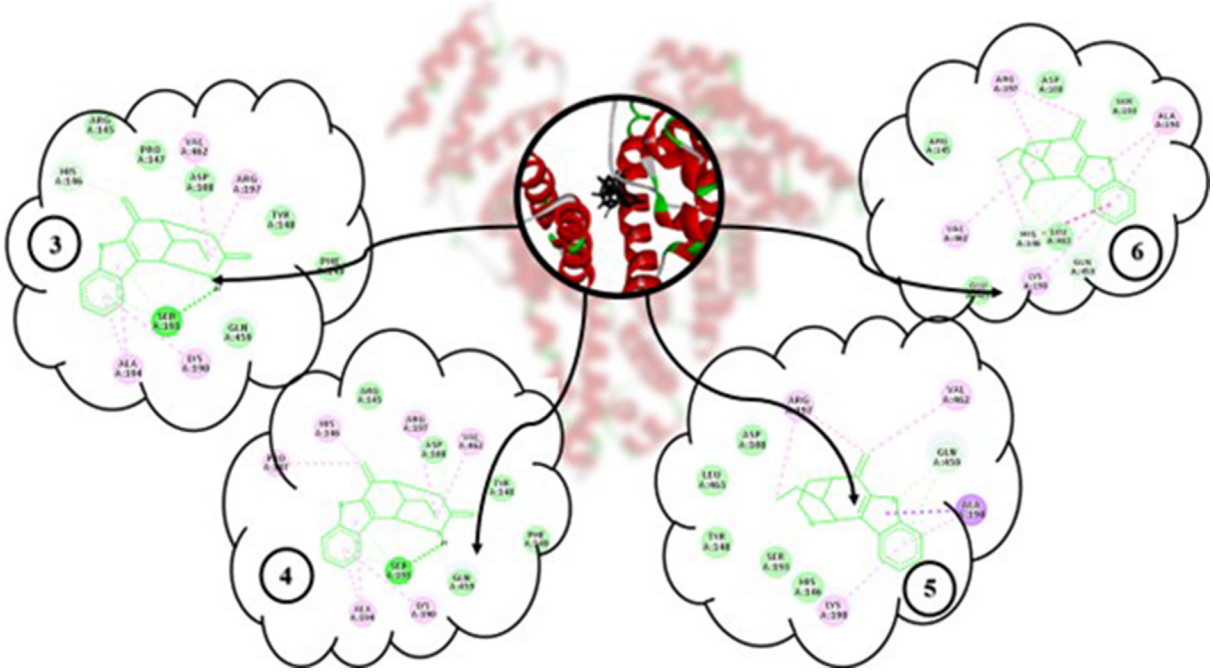

Figure 3. Interaction residue (middle), and interaction type of the molecules (**3–6**) with AChE crystal structure (turquoise and green: H-bonds; fuchsia: pi-interactions; pink: alkylic interactions; pale green: van der Waals).

both an advantage and a disadvantage. While weak binding affinity caused problems with transportation, strong interactions prevent to release of the active molecule in the target tissue [118]. Therefore, the interaction of uleine-derived molecules with HSA was also analyzed by using molecular docking methods and the results were compared with the results of tacrine and galantamine (Table 8). All molecules and drugs interacted with nearly the same region of the protein. **4** achieved the highest binding affinity with the contribution of alkylic interactions alongside one H-bond, while **6**, which had the lowest binding affinity, obtained two H-bonds with His146 and Gln459 (Figure S7).

3.6. Drug-likeness study

The molecular properties, drug-likeness analyses' results and scores of compounds **3–6** calculated by molinspiration [91] and Molsoft [92] tools were summarized in Table 9**.** Accordingly, the TPSA "topological polar surface area" scores [119] in $Å^2$ unit were calculated in order of **6** (19.03)< **5** (27.82)< **4** (44.89)< **3** (61.96) whereas the molecular volume (in $Å^3$) were determined in the following order **6** (265.86)> **4** (251.10)**>** **5** (248.98)> **3** (242.35). Also, the partition coefficient logP was determined as **6** (4.28)> **4** (4.04)**>** **5** (3.36)> **3** (2.52), which

Table 8. Active site analysis of crystal structure of SarA and BSA with silver complexes (blue: H-bond, purple: pi-interactions, red: alkyl interactions, black: van der Waals interactions).

Molecules	BA*	Amino Acids Residue
		AChE
3	-8.27	Ser203, Tyr337, Tyr124, Phe338, Trp86, Gly120, Gly121, Gly122, Tyr133, Glu202, Phe297, Gly448, Tyr449
4	-8.46	Gly122, Ser125, Gly122, Ser203, Trp86, Tyr124, His447, Tyr449, Asn87, Gly120, Gly121, Tyr133, Glu202
5	-8.52	Tyr124, Ser203, Tyr337, Trp86, Phe338, His447, Gly120, Gly121, Gly122, Tyr133, Glu202, Phe297
6	-8.66	Gly120, Tyr133, Tyr337, Trp86, His447, Gly121, Gly122, Tyr124, Ser125, Glu202, Ser203, Gly448
tacrine	-6.63	Tyr133, Glu202, Trp86, Tyr337, His447, Gly120, Gly121, Ser125, Gly126, Gly448, Ile451
galantamine	-7.75	Tyr124, Glu202, Ser203, Gly121, Trp86, Gly120, Gly122, Ser125, Phe297, Tyr337, Phe338, His447
BuChE		
3	-7.89	Trp82, Trp430, Tyr440, Phe329, Ala328, Tyr332, Asp70, Gly78, Glu197, His438, Gly439
4	-8.29	Trp82, Trp430, Tyr440, Phe329, Ala328, Tyr332, Asp70, Gly78, Glu197, His438, Gly439
5	-8.04	His438, Trp82, Phe329, Ala328, Tyr332, Asp70, Tyr128, Glu197, Trp430, Met437, Gly439, Tyr440
6	-8.15	His438, Trp82, Ala328, Tyr332, Trp430, Met437, Tyr440, Asp70, Ser79, Glu197, Phe329, Gly439
tacrine	-6.44	Gly115, Tyr128, Thr120, Trp82, His438, Gln97, Tyr114, Gly116, Gly121, Leu125, Glu197, Ile442
galantamine	-7.10	Glu197, Tyr440, Trp82, His438, Ala328, Trp430, Gly78, Tyr332, Phe329, Met437, Gly439, Ile442
HSA		
3	-7.38	Ser193, His146, Lys190, Ala194, Arg197, Val462, Asp108, Arg145, Pro147, Tyr148, Phe149, Gln459
4	-7.48	Ser193, His146, Pro147, Lys190, Ala194, Arg197, Val462, Asp108, Arg145, Tyr148, Phe149, Gln459
5	-6.85	Gln459, Ala194, Lys190, Arg197, Val462, Asp108, His146, Tyr148, Ser193, Leu463
6	-6.51	His146, Gln459, Lys190, Ala194, Arg197, Val462, Asp108, Arg145, Ser193, Glu425, Leu463
tacrine	-6.90	Tyr133, Glu202, Trp86, Tyr337, His447, Gly120, Gly121, Ser125, Gly126, Gly448, Ile451
galantamine	-6.78	His146, Ser193, Glu425, Ala194, Asp108, Arg145, Pro147, Tyr148, Lys190, Arg197, Gln459, Leu463

Table 9. Molecular properties, bioactivity and drug-likeness model scores.

	3	4	5	6
miLogP	2.52	3.36	4.04	4.28
TPSA (Å^2)	61.96	44.89	27.82	19.03
natoms	20	20	19	20
Molecular weight	268.32	266.34	252.36	266.39
nHBA	4	3	2	2
nHBD	2	2	2	1
nviolation	0	0	0	0
nrotb	1	1	1	1
Molecular volume (Å^3)	242.35	251.10	248.92	265.86
GPCR ligand	0.09	0.19	0.25	0.36
Ion channel modulator	-0.27	-0.07	0.27	0.34
Kinase inhibitor	-0.59	-0.46	-0.38	-0.26
Nuclear receptor ligand	-0.61	-0.20	-0.12	-0.08
Protease inhibitor	-0.17	-0.08	-0.18	-0.12
Enzyme inhibitor	-0.32	-0.08	-0.00	0.01
Drug-likeness model score	0.02	-0.30	-0.24	0.18

displayed that compound **6** could be a more lipophilic character than those of the others and thus could be absorbed at a higher rate and faster. The numbers of the HBA "H-Bond acceptor" and HBA "H-Bond donor" atoms (nitrogens and oxygens) were calculated as **6** (2) = **5** (2)< **4** (3) < **3** (4) and as **6** (1)< **5** (2) = **4** (2) = **3** (2), respectively. Considering the violation score of all compounds calculated as 0 (zero), all compounds can be a candidate for bio-pharmacological purposes because of agreeing with the Lipinski rules of 5 [120]. From Table 9, all compounds have certain activity scores for GPCR ligands, but compound **6** has the highest one. Namely, the biological activity scores of compounds against GPCR ligand were calculated as **6** (0.36)> **5** (0.25)> **4** (0.19)> **3** (0.09). Also, ion channel modulator scores for compounds **5** and **6** were calculated as 0.36 and 0.25, respectively, whereas this score for compounds **3** and **4** was calculated as -0.27 and -0.07. Considering the calculated molecular properties, drug-likeness and bioactivity scores, compound 6 can be said to be able to a promising candidate in future drug exploration.

4. Conclusions

As a result, the effectiveness of this route has been demonstrated by the efficient short synthesis of **(±)-**noruleine and **(±)-**uleine. This methodology was extended to other alkaloids and the broad family of natural products. This system is the first example of a one-pot construction of the tetracyclic 12-ethyl-1,2,3,4,5,6-hexahydro-1,5-methanoazocino [4,3-b]indole-3,6-dione (**3**) using TFB starting with 2-(3-ethyl-1-oxo-2,3,4,9-tetrahydro-1H-carbazol-2-yl)acetonitrile **1**. Especially, Ulein structure increases the importance of this study in AIDS and many similar medicinal applications. In this work, the synthesized molecules were charaterized by spectroscopic tools and they were compared with the calculated ones that were performed at B3LYP/6-311G(d,p) level and confirmed both structurally and spectroscopically. The results of the second-order perturbation energy analyses implied that the resonance interactions are mainly responsible for the lowering of the stabilization energy of the compound studied. AChE and BuChE inhibition activities of uleine derivative molecules were analyzed by molecular docking methods. All of the molecules had stronger interactions with approximately the same region of the enzymes than tacrine and galantamine. These results may give a conclusion that the studied and similar molecules may be candidates for choline esterase inhibitors. Additionally, the interaction results of molecules with HSA show both regional and energetic similarities with the results of tacrine and galantamine. The bioactivity and drug-likeness scores implied that compound **6** can be used for further drug-design studies more than the other molecules.

Declarations

Author contribution statement

Nesimi Uludag, Elvan Üstün, Goncagül Serdaroğlu: Conceived and designed the experiments; Performed the experiments; Analyzed and interpreted the data; Contributed reagents, materials, analysis tools or data; Wrote the paper.

Funding statement

Nesimi Uludag was supported by Scientific and Technological Research Council of Turkey [TUBITAK Project No.112T503].

Data availability statement

No data was used for the research described in the article.

Declaration of interests statement

The authors declare no conflict of interest.

Additional information

Supplementary content related to this article has been published online at https://doi.org/10.1016/j.heliyon.2022.e11990.

Acknowledgments

The authors thank Namık Kemal University for the analysis of our article structure. All calculations have been carried out at TUBITAK ULAKBIM, High Performance and Grid Computing Center (TR-Grid e-Infrastructure).

References

[1] H.M. Schmitt, S. Blechert, A new cationic domino process to (±)-Uleine, Angew. Chem. Int. Ed. Engl. 36 (1997) 1474–1476.
[2] J. Schmutz, F. Hunziker, R. Hirt, Ulein, das Hauptalkaloid von Aspidosperma ulei Mgf. Aspidosperma -Alkaloide, 1. Mitteilung, Helv. Chim. Acta 40 (1957) 1189–1200.
[3] M.-L. Bennasar, T. Roca, D. Garcia-Diaz, A New acyl radical based route to the 1,5-methanoazocino[4,3-b]indole framework of uleine and strychnos Alkaloids, J. Org. Chem. 73 (2008) 9033–9039.
[4] M. Ishikura, N. Takahashi, H. Takahashi, K. Yanada, Studies on the preparation of 1,5-methanoazocinoindole based on indolylborate, Heterocycles 66 (2005) 45–50.
[5] N. Uludag, A facile and convenient synthesis of (±)-dasycarpidone, Chem. Nat. Compd. 56 (2020) 105–108.
[6] J.A. Joule, M. Ohashi, B. Gilbert, C. Djerassi, Alkaloid studies- LIII. The structures of nine new alkaloids from aspidosperma dasycarpon A. DC, Tetrahedron 21 (1965) 1717–1734.
[7] Z.E.D.S. Torres, E.R. Silveira, L.F.R. e-silva, E.S. Lima, M.C. De Vasconcellos, D.E.D.A. Uchoa, R. Braz Filho, A.M. Pohlit, Chemical composition of aspidosperma ulei markgr. and antiplasmodial activity of selected indole alkaloids, Molecules 18 (2003) 6281–6297.
[8] P. Forns, A. Diez, M. Rubiralta, X. Solans, M. Font-Bardia, Synthetic applications of 2-(1,3-dithian-2-yl)indoles VI.1 Synthesis of 20-epidasycarpidone, Tetrahedron 52 (1996) 3563–3574.
[9] N. Uludag, An effective approach to the strychnos alkaloids: total synthesis of tubifolidine, Chem. Nat. Compd. 57 (2021) 491–496.
[10] N. Uludag, E. Duran, A New Approach to the total synthesis of 20-deethyltubifolidine and an entry to the azocino[4,3-b]indoles, Org. Prep. Proc. Int. 52 (2020) 434–441.
[11] P. Magnus, N.L. Sear, C.S. Kim, N. Vicker, Studies on the synthesis of Strychnos alkaloids. A new entry into the azocino[4,3-b]indole core structure and related studies, J. Org. Chem. 57 (1992) 70–78.
[12] C. Seidl, B.L. Correia, A.E.M. Stinghen, C.A.M. Santos, Z. Acetylcholinesterase, Inhibitory activity of uleine from Himatanthus lancifolius, Naturforscher C 65 (2010) 440–444.
[13] O.O. Franca, R.T. Brown, C.A.M. Santos, Uleine and demethoxyaspidospermine from the bark of Plumeria lancifolia, Fitoterapia 71 (208) (2000) 208–210.
[14] J.L. Cummings, Alzheimer's disease, N. Engl. J. Med. 351 (2004) 56–67.
[15] P. Francotte, P. De Tullio, P. Fraikin, B. Pirotte, In Search of novel AMPA potentiators, Med. Chem. 3 (2006) 239–246.

[16] T.P.C. Chierrito, A.C.C. Aguiar, I.M. de Andrade, I.P. Ceravolo, R.A.C. Goncalves, A. Jb de Oliveira, A. U Krettli, Anti-malarial activity of indole alkaloids isolated from Aspidosperma olivaceum, Malar. J. 13 (2014) 142.

[17] E.C. Miranda, S. Blechert, Gilbertin, ein neuer indolalkaloidtyp, Tetrahedron Lett 23 (1982) 5395–5398.

[18] D. Maes, R. Maes, Aspidosperma subincanum II. Usefulness of uleine and ribonucleic fragments in the treatment of AIDS patients, Rev. Bras. Farmcogn. 25 (2015) 42–46.

[19] J.-H. Shang, X.-H. Cai, T. Feng, Y.-L. Zhao, J.-K. Wang, L.-Y. Zang, M. Yan, X.-D. Luo, "Pharmacological evaluation of Alstonia scholaris: anti-inflammatory and analgesic effects", J. Ethnopharmacol. 129 (2010) 174–181.

[20] T.A. Reekie, M.G. Banwell, A.C. Willis, A raney-cobalt-mediated tandem reductive cyclization route to the 1,5-Methanoazocino[4,3-b]indole framework of the uleine and strychnos alkaloids, J. Org. Chem. 77 (2012) 10773–10781.

[21] D. Kim, J. H. Kim, T.-H. Jeon, C.-G. Cho, New synthetic routes to (+)-uleine and (−)-tubifolidine: general approach to 2-azabicyclo[3.3.1]nonane indole alkaloids, Org. Lett. 22 (2020) 3464–3468.

[22] S. Patir, N. Uludag, A novel synthetic route for the total synthesis of (±)-uleine, Tetrahedron 65 (2009) 115–118.

[23] N. Uludag, S. Patir, Studies on the synthesis of the azocino[4,3-b]indole framework and related compounds, J. Heterocycl. Chem. 44 (1317) (2007) 1317–1322.

[24] P. Magnus, N.L. Sear, C.S. Kim, N. Vicker, Studies on the synthesis of Strychnos alkaloids. A new entry into the azocino[4,3-b]indole core structure and related studies, J. Org. Chem. 57 (1992) 70–78.

[25] J. Jiricek, S. Blechert, Enantioselective synthesis of (−)-gilbertine via a cationic cascade cyclization, J. Am. Chem. Soc. 126 (2004) 3534–3538.

[26] C. Beemelmanns, H.-U. Reissig, A Short Formal total synthesis of strychnine with a samarium diiodide induced Cascade reaction as the key step, Angew. Chem., Int. Ed. 49 (2010) 8021–8025.

[27] N. Uludag, A new approach to the total synthesıs of (±)-nordasycarpıdone by rıng-closure wıth tetrachloro-1, 4-benzoquınone, Maced. J. Chem. Chem. En. 39 (11) (2020) 11–16.

[28] N. Uludag, M. Yakup, Concise total synthesis of 20-deethyl-4-demethyldasycarpidone, Org. Prep. Proc. Int. 47 (454) (2015) 454–460.

[29] J. Bonjoch, J. Quirante, M. Rodrigez, J. Bosch, Synthetic entry to 8-(o-nitrophenyl-2-azabicyclo[3.3.1]nonan-7-ones. Intermediates for the synthesis of strychnos-type systems, Tetrahedron 44 (1988) 2087–2092.

[30] M. Alvarez, R. Lavilla, J. Bosch, Studies on the synthesis of indole alkaloids. A direct entry to 4-ethylidene-hexahydro-1,5-methanoazocino[4,3-*b*]indoles, Tetrahedron Lett 28 (1987) 4457–4460.

[31] G. Serdaroglu, N. Uludag, Concise total synthesis of (±)-aspidospermidine and computational study: FT-IR, NMR, NBO, NLO, FMO, MEP diagrams, J. Mol. Struct. 1166 (2018) 286–303.

[32] W. He, P. Wang, J. Chen, W. Xie, Recent progress in the total synthesis of Strychnos alkaloids, Org. Biomol. Chem. 18 (2020) 1046–1056.

[33] N. Uludag, A concise total synthesis of ethylaspidospermidine, Org. Prep. Proc. Int. 51 (2019) 294–300.

[34] N. Uludag, T. Hokelek, S. Patir, A new approach to the total synthesis of (±)-20-epidasycarpidone, J. Heterocycl. Chem. 43 (2007) 585–591.

[35] J.N. Moorthy, N. Singal, Facile and highly selective conversion of nitriles to amides *via* indirect acid-catalyzed hydration Using TFA or AcOH−H_2SO_4, J. Org. Chem. 70 (2005) 1926–1929.

[36] S. Kumar, S.K. Dixit, S.K. Awasthi, An efficient one pot method for synthesis of carboxylic acids from nitriles using recyclable ionic liquid [bmim]HSO4, Tetrahedron Lett 55 (2014) 3802–3804.

[37] N. Uludag, M. Sanda, O. Asutay, N. Coskun, New route to 20-deethyldasycarpidone by ring-closure with DDQ, Org. Prep. Proc. Int. 46 (2014) 551–558.

[38] M.-L. Bennasar, T. Roca, D. Garcia-Diaz, A New Acyl radical-based route to the 1,5-methanoazocino[4,3-b]indole framework of uleine and strychnos alkaloids, J. Org. Lett. 73 (2008) 9033–9039.

[39] M. Feliz, J. Bosch, D. Mauleon, M. Amat, A.,A.J. Domingo, Synthetic applications of 2-cyano-1,2,3,6-tetrahydropyridines. Improved synthesis of the fundamental tetracyclic framework of dasycarpidone, J. Org. Chem. 47 (1982) 2435–2440.

[40] L.J. Doby, H. Biere, Total synthesis of (+-)-dasycarpidone, (+-)-epidasycarpidone, and (+-)-epiuleine, J. Org. Chem. 35 (1970) 3843–3845.

[41] R. Kuwano, M. Takahasaki, Y. Ito, Reduction of amides to amines *via* catalytic hydrosilylation by a rhodium complex, Tetrahedron Lett 48 (1998) 1017–1020.

[42] B. Ravinder, R.S. Rajeswar, A.R. Panasa, B. Rakeswar, Amide activation by TMSCl: reduction of amides to amines by LiAlH4 under mild conditions, Tetrahedron Lett 54 (4908) (2013) 4908–4913.

[43] F. Tang, M.G. Banwell, A.C. Willis, Palladium-catalyzed Ullmann cross-coupling/Tandem reductive cyclization route to key Members of the Uleine Alkaloid family, J. Org. Chem. 81 (2016) 2950–2957.

[44] N. Uludag, G. Serdaroglu, An improved synthesis, spectroscopic (FT-IR, NMR) study and DFT computational analysis (IR, NMR, UV–Vis, MEP diagrams, NBO, NLO, FMO) of the 1,5-methanoazocino[4,3-b]indole core structure, J. Mol. Struct. 1155 (2018) 548–560.

[45] N. Uludag, G. Serdaroglu, A. Yinanc, A novel synthesis of octahydropyrido[3,2-c] carbazole framework of aspidospermidine alkaloids and a combined computational, FT-IR, NMR, NBO, NLO, FMO, MEP study of the cis-4a-ethyl-1-(2hydroxyethyl)-2,3,4,4a,5,6,7,11c-octahydro-1H-pyrido[3,2-c]carbazole, J. Mol. Struct. 1161 (2018) 152–168.

[46] G. Serdaroglu, N. Uludag, P. Sugumar, P. Rajkumar, (-)-Tubifolidine as strychnos indole alkaloid: spectroscopic charactarization (FT-IR, NMR, UV-Vis), antioxidant activity, molecular docking, and DFT studies, J. Mol. Struct. 1244 (2021) 130978.

[47] P. Deshpande, N. Gogia, A. Singh, Exploring the efficacy of natural products in alleviating Alzheimer's disease, Neural. Regen. Res. 14 (8) (2019) 1321.

[48] A.I. Bush, The metallobiology of Alzheimer's disease, Trends Neurosci. 26 (4) (2003) 207–214.

[49] J.J. Jalbert, L.A. Daiello, K.L. Lapane, Dementia of the Alzheimer type, Epidemiol. Rev. 30 (1) (2008) 15–34.

[50] V.N. Talesa, Acetylcholinesterase in Alzheimer's disease, Mech. Ageing Dev. 122 (16) (2001) 1961–1969.

[51] G. Marucci, M. Buccioni, D. Dal Ben, C. Lambertucci, R. Volpini, F. Amenta, Efficacy of acetylcholinesterase inhibitors in Alzheimer's disease, Neuropharmacology 190 (2021), 108352.

[52] N.H. Greig, T. Utsuki, Q.-S. Yu, X. Zhu, H.W. Holloway, T. Perry, B. Lee, D.K. Ingram, D.K. Lahiri, A new therapeutic target in Alzheimer's disease treatment: attention to butyrylcholinesterase, Curr. Med. Res. Opin. 17 (3) (2001) 159–165.

[53] N. Dege, H. Gokce, O.E. Doğan, G. Alpaslan, Tuggan Agar, S. Muthu, Y. Sert, Quantum computational, spectroscopic investigations on N-(2-((2-chloro-4,5-dicyanophenyl)amino)ethyl)-4-methylbenzenesulfonamide by DFT/TD-DFT with different solvents, molecular docking and drug-likeness researches, Colloid. Surface. 638 (2022), 128311.

[54] A. Bielenica, S. Beegum, Y. Sheena Mary, Y. Shyma Mary, R. Thomas, S. Armakovic, S.J. Armakovic, S. Madeddu, M. Struga, V. Alsenoy, Experimental and computational analysis of 1-(4-chloro-3-nitrophenyl)-3-(3,4-dichlorophenyl) thiourea, J. Mol. Struct. 1205 (2020), 127587.

[55] S. Beegum, Y. Sheena Mary, Y. Shyma Mary, R. Thomas, S. Armakovic, S.J. Armakovic, J. Zitko, M. Dolezal, C. Van Alsenoy, Exploring the detailed spectroscopic characteristics, chemical and biological activity of two cyanopyrazine-2-carboxamide derivatives using experimental and theoretical tools, Spectrochim Acta A 224 (2020), 117414.

[56] M.A.A. Hay Allah, A.A. Balakit, H.I. Salman, A.A. Abdulridha, Y. Sert, New heterocyclic compound as carbon steel corrosion inhibitor in 1 M H2SO4, high efficiency at low concentration: experimental and theoretical studies, J. Adhes. Sci. Technol. (2022).

[57] A.A. Abdulridha, M.A.A. Hay Allah, S.Q. Makki, Y. Sert, H.E. Salman, A.A. Balakit, Corrosion inhibition of carbon steel in 1 M H2SO4 using new Azo Schiff compound: electrochemical, gravimetric, adsorption, surface and DFT studies, J. Mol. Liq. 315 (2020), 113690.

[58] A.A. Balakit, S.Q. Makkib, Y. Sert, F. Ucune, M.B. Alshammarif, P. Thordarsong, G.A. El-Hiti, Synthesis, spectrophotometric and DFT studies of new Triazole Schiff bases as selective naked-eye sensors for acetate anion, Supramol. Chem. 32 (10) (2022) 519–526.

[59] H. Gökce, S. Ceylan, N. Öztürk, Y. Sert, Tautomeric, spectroscopic, electronic and NLO analyses of purpald (4-amino-3-hydrazino-5-mercapto-1,2,4-triazole), Mater. Today Commun. 32 (2022), 103862.

[60] A.D. Becke, A new mixing of Hartree–Fock and local density-functional theories, J. Chem. Phys. 98 (1993) 1372–1377.

[61] C. Lee, W. Yang, R.G. Parr, Development of the Colle-Salvetti correlation-energy formula into a functional of the electron density, Phys. Rev. B37 (1988) 785–789.

[62] K. Raghavachari, J.S. Binkley, R. Seeger, J.A. Pople, Self-Consistent molecular orbital methods. 20. Basis set for correlated wave-functions, J. Chem. Phys. 72 (1980) 650–654.

[63] A.D. McLean, G.S. Chandler, Contracted Gaussian-basis sets for molecular calculations. 1. 2nd row atoms, Z=11-18, J. Chem. Phys. 72 (1980) 5639–5648.

[64] M.J. Frisch, J.A. Pople, J.S. Binkley, Self-Consistent molecular orbital methods. 25. Supplementary functions for Gaussian basis sets, J. Chem. Phys. 80 (1984) 3265–3269.

[65] M. Cossi, V. Barone, R. Cammi, J. Tomasi, Ab initio study of solvated molecules: a new implementation of the polarizable continuum model, Chem. Phys. Lett. 255 (1996) 327–335.

[66] J. Tomasi, B. Mennucci, R. Cammi, Quantum mechanical continuum solvation models, Chem. Rev. 105 (2005) 2999–3093.

[67] S. Miertuš, E. Scrocco, J. Tomasi, Electrostatic interaction of a solute with a continuum. A direct utilization of ab initio molecular potentials for the prevision of solvent effects, Chem. Phys. 55 (1981) 117–129.

[68] X. Li, M.J. Frisch, Energy-represented DIIS within a hybrid geometry optimization method, J. Chem. Theor. Comput. 2 (2006) 835–839.

[69] K.N. Kudin, G.E. Scuseria, E. Cancès, A black-box self-consistent field convergence algorithm: one step closer, J. Chem. Phys. 116 (2002) 8255–8261.

[70] M.J. Frisch, G.W. Trucks, H.B. Schlegel, G.E. Scuseria, M.A. Robb, J.R. Cheeseman, G. Scalmani, V. Barone, B. Mennucci, G.A. Petersson, H. Nakatsuji, M. Caricato, X. Li, H.P. Hratchian, A.F. Izmaylov, J. Bloino, G. Zheng, J.L. Sonnenberg, M. Hada, M. Ehara, K. Toyota, R. Fukuda, J. Hasegawa, M. Ishida, T. Nakajima, Y. Honda, O. Kitao, H. Nakai, T. Vreven, J.A. Montgomery Jr., J.E. Peralta, F. Ogliaro, M. Bearpark, J.J. Heyd, E. Brothers, K.N. Kudin, V.N. Staroverov, T. Keith, R. Kobayashi, J. Normand, K. Raghavachari, A. Rendell, J.C. Burant, S.S. Iyengar, J. Tomasi, M. Cossi, N. Rega, J.M. Millam, M. Klene, J.E. Knox, J.B. Cross, V. Bakken, C. Adamo, J. Jaramillo, R. Gomperts, R.E. Stratmann, O. Yazyev, A.J. Austin, R. Cammi, C. Pomelli, J.W. Ochterski, R.L. Martin, K. Morokuma, V.G. Zakrzewski, G.A. Voth, P. Salvador, J.J. Dannenberg, S. Dapprich, A.D. Daniels, O. Farkas, J.B. Foresman, J.V. Ortiz, J. Cioslowski, D.J. Fox, Gaussian 09W, *Revision D.01*, Gaussian, Inc, Wallingford CT, 2013.

[71] GaussView 6.0.16, Gaussian, Inc, Wallingford CT, 2016.

[72] D.A. McQuarrie, Statistical Thermodynamics, Harper & Row Publishers, New York, 1973.

[73] T.L. Hill, An Introduction to Statistical Thermodynamics, Addison- Wesley Publishing, Inc, London, 1962.

[74] G. Herzberg, Molecular Spectra and Molecular Structure III,1, Edition, D. Van Nostrand Company, Inc., New York, 1964.

[75] G. Serdaroglu, S. Durmaz, DFT and statistical mechanics entropy calculations of diatomic and polyatomic molecules, Indian J. Chem. 49 (2010) 861–866.
[76] T. Koopmans, Über die Zuordnung von Wellenfunktionen und Eigenwertenzu den Einzelnen Elektronen Eines Atoms, Physica 1 (1934) 104–113.
[77] J.P. Perdew, R.G. Parr, M. Levy, J.L. Balduz, Density-functional theory for fractional particle number: derivative discontinuities of the energy, Phys. Rev. Lett. 49 (23) (1982) 1691–1694.
[78] J.F. Janak, Proof that $\partial E/\partial_{ni}=\varepsilon i_n$ density-functional theory, Phys. Rev. B 18 (12) (1978) 7165–7168.
[79] J.P. Perdew, M. Levy, Physical content of the exact Kohn-Sham orbital energies: band gaps and derivative discontinuities, Phys. Rev. Lett. 51 (20) (1983) 1884–1887.
[80] R.G. Parr, R.G. Pearson, Absolute hardness*: companion parameter to absolute electronegativity"*, J. Am. Chem. Soc. 105 (1983) 7512–7516.
[81] R.G. Pearson, Absolute electronegativity and hardness correlated with molecular orbital theory, *Proc. Natl. Acad. Sci.* USA 83 (1986) 8440–8441.
[82] R.G. Parr, L.V. Szentpaly, S. Liu, Electrophilicity index, J. Am. Chem. Soc. 121 (1999) 1922–1924.
[83] J.L. Gazquez, A. Cedillo, A. Vela, Electrodonatingand electroaccepting powers, J. Phys. Chem. A 111 (10) (2007) 1966–1970.
[84] B. Gomez, N.V. Likhanova, M.A. Domínguez-Aguilar, R. Martínez-Palou, A. Vela, J.L. Gazquez, Quantum chemical study of the inhibitive properties of 2-pyridyl-azoles, J. Phys. Chem. B 110 (18) (2006) 8928–8934.
[85] J.P. Foster, F. Weinhold, Natural hybrid orbitals, J. Am. Chem. Soc. 102 (1980) 7211–7218.
[86] A.E. Reed, R.B. Weinstock, F. Weinhold, Natural-population analysis, J. Chem. Phys. 83 (1985) 735–746.
[87] A.E. Reed, F. Weinhold, Natural localized molecular orbitals, J. Chem. Phys. 83 (1985) 1736–1740.
[88] A. E. Reed, L. A. Curtiss, F. Weinhold, "Intermolecular Interactions from a Natural Bond Orbital, donor-acceptor viewpoint.
[89] K. Wolinski, J.F. Hinton, P. Pulay, Efficient implementation of the gauge-independent atomic orbital method for NMR chemical shift calculations, J. Am. Chem. Soc. 112 (23) (1990) 8251–8260.
[90] J.R. Cheeseman, G.W. Trucks, T.A. Keith, M.J. Frisch, A comparison of models for calculating nuclear magnetic resonance shielding tensors, J. Chem. Phys. 104 (1996) 5497–5509.
[91] https://www.molinspiration.com.
[92] https://molsoft.com/mprop.
[93] H. Dvir, I. Silman, M. Harel, T.L. Rosenberry, J.L. Sussman, Acetylcholinesterase: from 3D structure to function, Chem. Biol. Interact. 187 (1-3) (2010) 10–22.
[94] Y. Nicolet, O. Lockridge, P. Masson, J.C. Fontecilla-Camps, F. Nachon, Crystal structure of human butyrylcholinesterase and of its complexes with substrate and products, J. Biol. Chem. 278 (42) (2003) 41141–41147.
[95] S. Sugio, A. Kashima, S. Mochizuki, M. Noda, K. Kobayashi, Crystal structure of human serum albumin at 2.5 Å resolution, Protein Eng 12 (6) (1999) 439–446.
[96] J. Wang, P. Morin, W. Wang, P.A. Kollman, Use of MM-PBSA in reproducing the binding free energies to HIV-1 RT of TIBO derivatives and predicting the binding mode to HIV-1 RT of efavirenz by docking and MM-PBSA, J. Am. Chem. Soc. 123 (22) (2001) 5221–5230.
[97] O. Trott, A.J. Olson, AutoDock Vina, Improving the speed and accuracy of docking with a new scoring function, efficient optimization, and multithreading, J. Comput. Chem. 31 (2) (2010) 455–461.
[98] G. Serdaroğlu, N. Şahin, E. Üstün, M.N. Tahir, C. Arıcı, N. Gürbüz, İ. Özdemir, PEPPSI type complexes: synthesis, x-ray structures, spectral studies, molecular docking and theoretical investigations, Polyhedron 204 (2021), 115281.
[99] N. Uludağ, G. Serdaroğlu, P. Sugumar, P. Rajkumar, N. Çolak, E. Erçağ, Synthesis of thiophene derivatives: substituent effect, antioxidant activity, cyclic voltammetry, molecular docking, DFT, and TD-DFT calculations, J. Mol. Struct. 1257 (2022), 132607.
[100] M.P. Andersson, P. Uvdal, New Scale Factors for Harmonic Vibrational Frequencies Using the B3LYP Density Functional Method with the Triple-ζ Basis Set 6–311+G(d,p), J. Phys. Chem. 109 (2005) 2937–2941.
[101] B. Tercan, E. Şahin, S. Patır, T. Hökelek, 2-Ethyl-6,6-ethylenedisulfanediyl-7-methoxymethyl-1,2,3,4,5,6-hexahydro-1,5-methanoazocino[4,3-b]indol-3-one, Acta Crystallogr. E66 (2010) o328.
[102] B. Tercan, F. Yüksel, S. Patır, T. Hökelek, 6,6-[Ethylenebis(sulfanediyl)]-2-(2-methoxyethyl)-1,2,3,4,5,6-hexahydro-1,5-methano-1H-azocino[4,3-b]indol-3-one, Acta Crystallogr. E66 (2010) o1275–o1276.
[103] N.A. Mangalama, M.R.P. Kurup, E. Suresh, S. Kaya, G. Serdaroğlu, Diversities in the chelation of aroylhydrazones towards cobalt(II) salts: synthesis, spectral characterization, crystal structure and some theoretical studies, J. Mol. Struct. 1232 (2021), 129978.
[104] J.S. Al-Otaibi, Y.S. Mary, Y.S. Mary, G. Serdaroglu, Adsorption of adipic acid in Al/B-N/P nanocages: DFT investigations, "Adsorption of adipic acid in Al/B-N/P nanocages: DFT investigations", J. Mol. Model. 27 (2021) 113.
[105] G. Serdaroğlu, A computational study on relationship between quantum chemical parameters and reactivity of the zwitterionic GABA and its agonists: solvent effect, Indian J. Chem. A. 56A (11) (2017) 1143–1153.
[106] M. Elik, G. Serdaroğlu, A computational study of 1-substituted methyl 9-methyl-9H-Pyrido[3,4- b]indole-3-carboxylate: quantum chemical descriptors, FMO and NBO analysis, Cumhuriyet Sci. J. 38 (4) (2017) 138–155.
[107] M. Erdoğan, G. Serdaroğlu, New hybrid (E)-4-((pyren-1-ylmethylene)amino)-N-(thiazol-2-yl)benzenesulfonamide as a potential drug candidate: spectroscopy, TD-DFT, NBO, FMO, and MEP studies, ChemistrySelect 6 (2021) 9369–9381.
[108] D. Muñoz-Torrero, P. Camps, Huprines for Alzheimer's disease drug development, Expet Opin. Drug Discov. 3 (1) (2008) 65–81.
[109] B. Truong, J.P. Quiroz, R. Priefer, Acetylcholinesterase inhibitors for Alzheimer's disease: past, present, and potential future, Med. Res. Arch. 8 (11) (2020).
[110] F. Zhang, K. Zhao, T. Tang, Y. Deng, Y. Zhang, S. Feng, P. Feng, M. Guo, X. Li, J. Cen, Bisindole compound 4ae ameliorated cognitive impairment in rats with vascular dementia by anti-inflammation effect via microglia cells, Eur. J. Pharmacol. 908 (2021), 174357.
[111] X. Jin, M. Wang, J. Shentu, C. Huang, Y. Bai, H. Pan, D. Zhang, Z. Yuan, H. Zhang, X. Xiao, X. Wu, L. Ding, Q. Wang, S. He, W. Cui, Inhibition of acetylcholinesterase activity and β-amyloid oligomer formation by 6-bromotryptamine A, a multi-target anti-Alzheimer's molecule, Oncol. Lett. 19 (2) (2020) 1593–1601.
[112] S. Burmaoglu, E.A. Kazancioglu, M.Z. Kazancioglu, R. Sağlamtaş, G. Yalcin, I. Gulcin, O. Algul, Synthesis, molecular docking and some metabolic enzyme inhibition properties of biphenyl-substituted chalcone derivatives, J. Mol. Struct. 1254 (2022), 132358.
[113] A. Ahmed, S. Akhtar, N. Mushtaq, S. Haider, R. Munawar, H.A. Siddique, A. Akram, Z.S. Saif, M. Arif, 1, 3-di-4-piperidylpropane derivatives as potential acetyl cholinesterase antagonists: molecular docking, synthesis, and biological evaluation, Pak. J. Pharm. Sci. 34 (3) (2021) 855–860.
[114] M.R. Islam, A. Zaman, I. Jahan, R. Chakravorty, S. Chakraborty, In silico QSAR analysis of quercetin reveals its potential as therapeutic drug for Alzheimer's disease, J. Young Pharm. 5 (4) (2013) 173–179.
[115] I. Celik, M. Erol, Ö.T. Arpaci, F.S. Senol, I.E. Orhan, Evaluation of activity of some 2, 5-disubstituted benzoxazole derivatives against acetylcholinesterase, butyrylcholinesterase and tyrosinase: ADME prediction, DFT and comparative molecular docking studies, Polycycl. Aromat. Comp. 42 (2) (2022) 412–423.
[116] D.C. Carter, J.X. Ho, Structure of serum albumin, Adv. Protein Chem. 45 (1994) 153–203.
[117] Y. Ishima, T. Maruyama, Human serum albumin as carrier in drug delivery systems, Yakugaku Zasshi- J. Pharm. Soc. Japan. 136 (1) (2016) 39–47.
[118] A.M. Merlot, D.S. Kalinowski, D.R. Richardson, Unraveling the mysteries of serum albumin—more than just a serum protein, Front. Physiol. 5 (2014) 299.
[119] P. Ertl, B. Rohde, P. Selzer, Fast calculation of molecular polar surface area as a sum of fragment-based contributions and its application to the prediction of drug transport properties, J. Med. Chem. 43 (2000) 3714–3717.
[120] C.A. Lipinski, F. Lombardo, B.W. Dominy, P.J. Feeney, Experimental and computational approaches to estimate solubility and permeability in drug discovery and development settings, Adv. Drug Deliv. Rev. 23 (1–3) (1997) 3–25.